

CANCER

Chemical induction of splice-neoantigens attenuates tumor growth in a preclinical model of colorectal cancer

Shingo Matsushima^{1,2,3}, Masahiko Ajiro^{1,2*}, Kei Iida^{4,5}, Kenji Chamoto⁶, Tasuku Honjo⁶, Masatoshi Hagiwara^{1,2*}

Copyright © 2022
The Authors, some
rights reserved;
exclusive licensee
American Association
for the Advancement
of Science. No claim
to original U.S.
Government Works

Neoantigen production is a determinant of cancer immunotherapy. However, the expansion of neoantigen abundance for cancer therapeutics is technically challenging. Here, we report that the synthetic compound RECTAS can induce the production of splice-neoantigens that could be used to boost antitumor immune responses. RECTAS suppressed tumor growth in a CD8⁺ T cell– and tumor major histocompatibility complex class I–dependent manner and enhanced immune checkpoint blockade efficacy. Subsequent transcriptome analysis and validation for immunogenicity identified six splice-neoantigen candidates whose expression was induced by RECTAS treatment. Vaccination of the identified neopeptides elicited T cell responses capable of killing cancer cells *in vitro*, in addition to suppression of tumor growth *in vivo* upon sensitization with RECTAS. Collectively, these results provide support for the further development of splice variant–inducing treatments for cancer immunotherapy.

INTRODUCTION

The immune surveillance system protects individuals from the emergence of cancer cells due to intrinsic or extrinsic causes (1, 2). Cancer cells, however, often evade immune responses through the expression of programmed cell death ligand 1 (PD-L1) (3); thus, the use of immune checkpoint inhibitors (ICIs) targeting PD-L1 or its receptor, programmed cell death 1 (PD-1), revolutionized cancer therapeutics when they were first approved in 2014 for the treatment of patients with melanoma (4, 5). Although ICIs have markedly improved the survival rate of patients with cancer compared with other treatment approaches, a substantial number of patients show poor response or resistance to PD-1 blockade therapies (6, 7). Meta-analyses for PD-1 blockade responses highlight the importance of neoantigens, derived from nonsynonymous mutations in cancer cells, for antitumor immune responses (8, 9). Recent transcriptome and genomics studies by The Cancer Genome Atlas and others predict the presence of putative neoantigens as a result of an irregular pre-mRNA splicing regulation in cancer cells (10, 11). Peptides from aberrant splicing were actually presented on major histocompatibility complex (MHC) class I in cancer cell lines (12). In addition, T cell activation by aberrant splicing–derived peptides has subsequently been reported (13, 14), indicating that alterations in RNA splicing in cancer cells might induce antitumor immune responses.

Previously, we developed small-molecule splicing modulators, which suppress (15) or promote (16) the activity of serine/

arginine-rich splicing factors (SRSFs) by targeting CDC-like kinases (CLKs). Their therapeutic potential has been successfully demonstrated for genetic diseases such as Duchenne muscular dystrophy (17), anhidrotic ectodermal dysplasia with immunodeficiency (18), cystic fibrosis (19), Parkinson's disease (20), and familial dysautonomia (16, 21). In our recent study on the role of *IKBKAP* splicing mutation in familial dysautonomia, we demonstrated that RECTAS induced exon 20 recognition in an SRSF6-dependent manner (16). Here, we report that RECTAS promotes tumor immunogenicity through induction of splice-neoantigens, whose antitumor effects were validated *ex vivo* and *in vivo*, paving the way toward translational application for cancer immunotherapy.

RESULTS

The splice modifier RECTAS exhibited CD8⁺ T cell–dependent antitumor effects and potentiated the response to PD-1 blockade

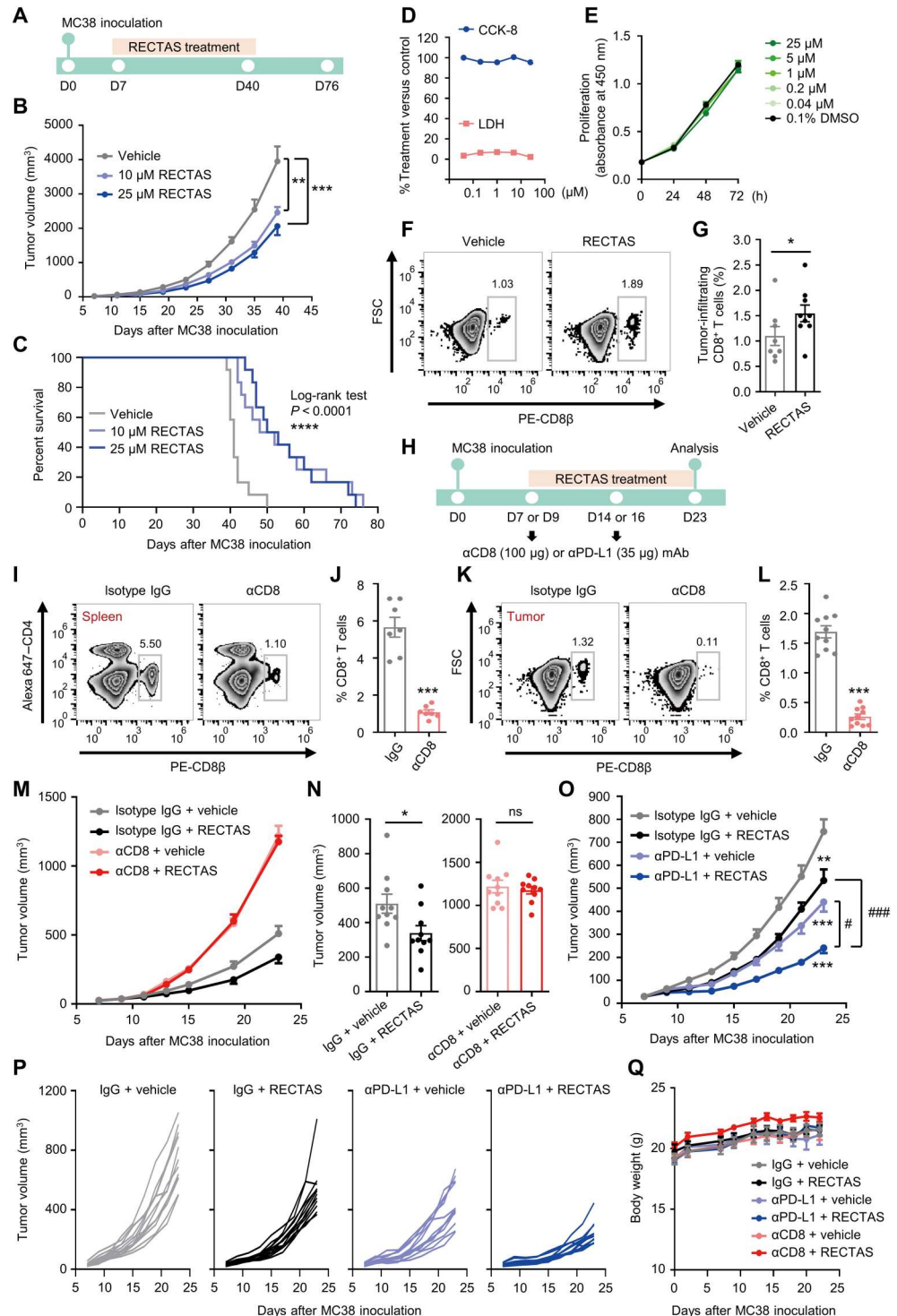
To investigate whether the small-molecule splice modifiers that we previously reported, CLK inhibitor CaNDY (19) and CLK activator RECTAS (16), have antitumor effects, we assessed their activity *in vivo* with intradermally transplanted syngeneic MC38 tumors in immunocompetent mice (Fig. 1A). RECTAS resulted in the suppression of tumor growth *in vivo* and prolonged the survival (Fig. 1, B and C, and fig. S1A) at a concentration that was not associated with cytotoxicity or cytostasis *in vitro* (Fig. 1, D and E, and fig. S1B), whereas CaNDY did not (fig. S1, C to F). By analyzing extracted tumors, we found that the frequency of tumor-infiltrating CD8⁺ T cells was increased to about 1.5-fold after RECTAS treatment (Fig. 1, F and G).

These observations prompted us to examine whether the RECTAS-induced antitumor effect was due to enhanced tumor immunity. Thus, we next conducted depletion of endogenous CD8⁺ T cells with CD8-depleting antibody (α CD8) and evaluated the antitumor effect of RECTAS administration (Fig. 1H). A depletion of greater than 80% CD8⁺ T cells was achieved in the spleen (Fig. 1,

¹Department of Anatomy and Developmental Biology, Kyoto University Graduate School of Medicine, Kyoto 606-8501, Japan. ²Department of Drug Discovery Medicine, Kyoto University Graduate School of Medicine, Kyoto 606-8507, Japan. ³Pharmacology Research Laboratories, Watarase Research Center, Kyorin Pharmaceutical Co. Ltd, Tochigi 329-0114, Japan. ⁴Medical Research Support Center, Kyoto University Graduate School of Medicine, Kyoto 606-8501, Japan. ⁵Faculty of Science and Engineering, Kindai University, Osaka 577-8502, Japan. ⁶Department of Immunology and Genomic Medicine, Center for Cancer Immunotherapy and Immunobiology, Kyoto University Graduate School of Medicine, Kyoto 606-8501, Japan.

*Corresponding author. Email: ajiro.masahiko.6e@kyoto-u.ac.jp (M.A.); hagiwara.masatoshi.8c@kyoto-u.ac.jp (M.H.)

Fig. 1. Chemical activation of SRSFs exerts antitumor effects in a CD8⁺ T cell-dependent manner and potentiates the response to PD-1 blockade. (A) Experimental procedure for the MC38 tumor-bearing model. (B and C) Tumor volumes (B) and survival (C) are shown ($n = 12$ per group). ** $P < 0.01$ and *** $P < 0.001$. (D and E) MC38 cells were treated with RECTAS for 72 hours (D) or for the indicated time (E); cell proliferation and cell death were measured using CCK-8 and lactate dehydrogenase (LDH) assays, respectively ($n = 3$ per group). (F and G) Representative images (F) and quantitative data (G) of FCM are shown ($n = 8$ to 9 per group). * $P < 0.05$. FSC, forward scatter; PE, phycoerythrin. (H) Experimental procedure of antibody injection in an MC38 tumor-bearing model. (I to L) Representative images (I and K) and quantitative data (J and L) of FCM are shown [$n = 7$ per group for spleen (J); $n = 10$ per group for tumor (L)]. *** $P < 0.001$. (M and N) Tumor growth curve (M) and tumor volumes on day 23 (N) are shown ($n = 10$ per group). * $P < 0.05$. ns, not significant. (O and P) Tumor volumes of mice ($n = 12$ per group) are shown collectively (O) or individually (P). ** $P < 0.01$ and *** $P < 0.001$ versus isotype IgG + vehicle; # $P < 0.05$ and ### $P < 0.001$ between the indicated groups. (Q) Changes in body weight of mice are shown ($n = 5$ per group). All data are shown as means \pm SEM. All experiments were performed at least twice. Statistical significance was determined using an unpaired Student's t test for (G), (J), (L), and (N) and one-way ANOVA followed by Bonferroni's multiple comparisons test for (B) and (O).



I and J) and tumor (Fig. 1, K and L); we found that RECTAS administration was not effective for tumor suppression when CD8⁺ T cells were depleted (Fig. 1, M and N, and fig. S1G). The antitumor activity of RECTAS in the MC38 tumor-bearing model was thus attributed to an enhanced CD8⁺ T cell-mediated immune response.

As tumor immunogenicity has been associated with clinical responses to PD-1 blockade, we investigated whether RECTAS

treatment enhances the antitumor effects of anti-PD-L1 antibody (α PD-L1). We found that RECTAS on its own suppressed tumor growth by 28.5% [isotype immunoglobulin G (IgG) + vehicle versus isotype IgG + RECTAS, $P = 1.1 \times 10^{-3}$], whereas α PD-L1 suppressed tumor growth by 41.0% (isotype IgG + vehicle versus α PD-L1 + vehicle, $P \leq 1.0 \times 10^{-4}$) on day 23 (Fig. 1, O and P); thus, a tumor suppression of about 57.8% is expected when

RECTAS and α PD-L1 function additively. However, we observed tumor suppression by 67.8% when RECTAS and α PD-L1 were co-administered (isotype IgG + vehicle versus α PD-L1 + RECTAS, $P \leq 1.0 \times 10^{-4}$), suggesting that they function in an additive, or possibly synergistic, manner (Fig. 1, O and P). Flow cytometry (FCM) also revealed an increase in the number of tumor-infiltrating CD8⁺ T cells in groups cotreated with RECTAS and α PD-L1, compared to those treated with α PD-L1 alone (fig. S1H). In addition, we confirmed that collected tumor mass correlated well with measured tumor volumes in these experiments (fig. S1, I and J). There was no change in the body weight or apparent adverse effects in mice treated with isotype IgG, α PD-L1, or α CD8, with or without RECTAS (Fig. 1Q). These results indicated that RECTAS-induced chemical activation of SRSFs exerts antitumor effects in a CD8⁺ T cell-dependent manner and improves the efficacy of PD-1 blockade without direct cytotoxic or cytostatic effects on cancer cells.

RECTAS enhanced tumor immunogenicity without antigen-independent activation of T cells or autoimmune responses

Alterations in the production of splice isoforms during T cell activation likely affect the subsequent functions (22). Given that RECTAS exerted antitumor effects in a CD8⁺ T cell-dependent manner, we next determined whether RECTAS induced antigen-independent activation of T cells using an ex vivo splenocyte culture assay. We first isolated splenocytes from normal mice, and cells were treated with RECTAS for 24 hours (Fig. 2A). We then measured the frequencies of the CD44⁺ effector T cell marker and CD69⁺ acute T cell activation marker in CD8⁺ or CD4⁺ T cells using FCM (Fig. 2, B and C). As expected, treatment with concanavalin A promoted both CD44⁺ and CD69⁺ marker expressions in CD8⁺ and CD4⁺ T cells, whereas treatment with RECTAS had no such effects (Fig. 2, C to E, and fig. S2A). We did not observe any secretion of inflammatory cytokines, including interferon- γ (IFN- γ) and tumor necrosis factor- α (TNF- α), in the RECTAS-treated group (Fig. 2, F and G). These results excluded the involvement of antigen-independent activation of T cells after administration of RECTAS.

Next, to determine whether the enhanced tumor immunity upon coadministration of RECTAS and α PD-L1 raises concerns regarding autoimmune reactions, we systemically administered a high dose of RECTAS in normal mice for 7 or 28 days (Fig. 2H). With respect to the acute response on day 7, we confirmed that RECTAS administration with or without α PD-L1 had no effect on the leukocyte numbers, spleen weights, and expression of T cell activation markers (CD44^{high}CD8⁺, CD69⁺CD8⁺, CD44^{high}CD4⁺, or CD69⁺CD4⁺) in the peripheral blood and spleen (Fig. 2, I and J, and fig. S2, B and C). Moreover, body weight changes were found to be comparable in all groups throughout the experimental period (Fig. 2K), and histological analysis of nonmalignant tissues obtained on day 28 revealed that chronic exposure of normal mice to RECTAS did not result in the accumulation of CD8⁺ T cells or appearance of inflammatory lesions, irrespective of cotreatment with α PD-L1 (Fig. 2, L and M, and fig. S2D). In addition, no alterations were observed in leukocyte numbers and biochemical parameters in peripheral blood (fig. S2, E and F, and data file S1). These results indicated that RECTAS enhanced tumor immunogenicity without overt adverse inflammatory or autoimmune reactions.

MHC class I in cancer cells was indispensable for the antitumor effect of RECTAS

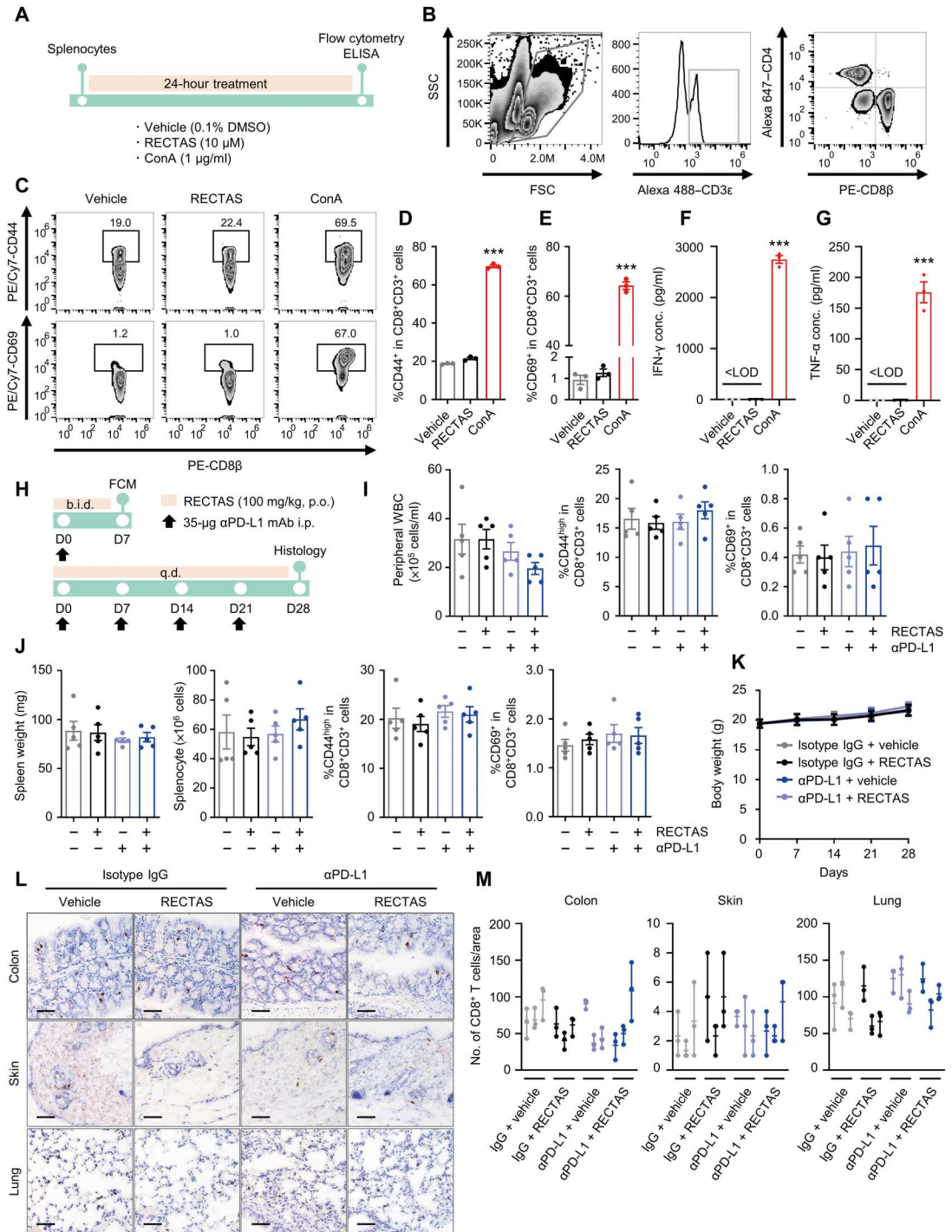
MHC class I expressed by cancer cells is critical for neoantigen presentation, which is indispensable for CD8⁺ T cell-dependent immune surveillance and tumor killing (5, 6). To investigate whether RECTAS modulated the neoantigen presentation pathway, we first examined the effects of RECTAS on IFN- γ signaling and the expression of MHC class I components, including β 2-microglobulin (B2M) and H2-K^b in MC38 cells, because CD8⁺ T cell-secreted IFN- γ is a major inducer of MHC class I components (fig. S3A) (23). Treatment with IFN- γ robustly induced the phosphorylation of signal transducer and activator of transcription 1 (STAT1) and STAT3 and increased expression of the B2M protein, whereas administration of RECTAS had no such effects (fig. S3B). We also found a slight increase in H2-K^b expression (11.1 and 12.4% at IFN- γ concentrations of 0 and 0.1 ng/ml for 72 hours; fig. S3C) and a decrease in PD-L1 expression on the cell surface (3.8, 3.2, and 26.1% at IFN- γ concentrations of 0, 0.1, and 1 ng/ml for 72 hours; fig. S3D). In contrast, we did not detect any changes in the expression of PD-L1 in host dendritic cells or macrophages (fig. S3E). According to the RNA sequencing (RNA-seq) data (fig. S4), mRNA expression and splicing patterns of H2-K^b and PD-L1 were not altered in MC38 cells after treatment with RECTAS; therefore, we attributed these alterations to posttranslational regulation. However, these modest alterations were likely not the functional mechanisms through which RECTAS exerts its antitumor effects, as we observed enhanced antitumor effect of RECTAS when coadministered with α PD-L1 (Fig. 1, O and P).

We further investigated whether neoantigen presentation in cancer cells is important for the antitumor effects of RECTAS by establishing a CRISPR-Cas9-mediated knockout (KO) of *B2m*, the essential component of MHC class I, using MC38 cells. The resulting *B2m*-KO MC38 clones (*B2m* KO #1 and #2) exhibited a complete loss of endogenous *B2m* (Fig. 3A), without affecting cell proliferation (Fig. 3B). We further confirmed the loss of surface H2-K^b on these cells (Fig. 3, C and D), without affecting IFN- γ signaling through STAT1 phosphorylation (Fig. 3A) or expression of PD-L1 on the cell surface (Fig. 3, E and F). Then, we intradermally inoculated these *B2m* KO MC38 clones into immunocompetent mice and evaluated the antitumor effect of RECTAS treatment (Fig. 3G). Treatment with RECTAS consistently suppressed tumor growth in the negative control clone, whereas this effect was completely abolished in *B2m* KO clones (Fig. 3H). Moreover, the number of CD8⁺ T cells was lower in *B2m* KO tumors, consistent with the essential role of tumor-expressed MHC class I in promoting T cell proliferation (24) and was no longer inducible by treatment with RECTAS in *B2m* KO-derived tumors (Fig. 3, I and J). We also confirmed the antitumor effect of α PD-L1 in the negative control clone, but not in the *B2m* KO clone (Fig. 3K). These results indicate that in cancer cells, MHC class I plays a crucial role in determining the antitumor effects of RECTAS.

Identification of potential splice-neoantigens inducible by RECTAS administration

After confirming that MHC class I expressed by cancer cells was indispensable for the antitumor effects of RECTAS, we hypothesized that RECTAS treatment could alter aberrant pre-mRNA alternative splicing events and enhance the production of splice-neoantigens (Fig. 4A). We thus performed RNA-seq analysis to assess RNA

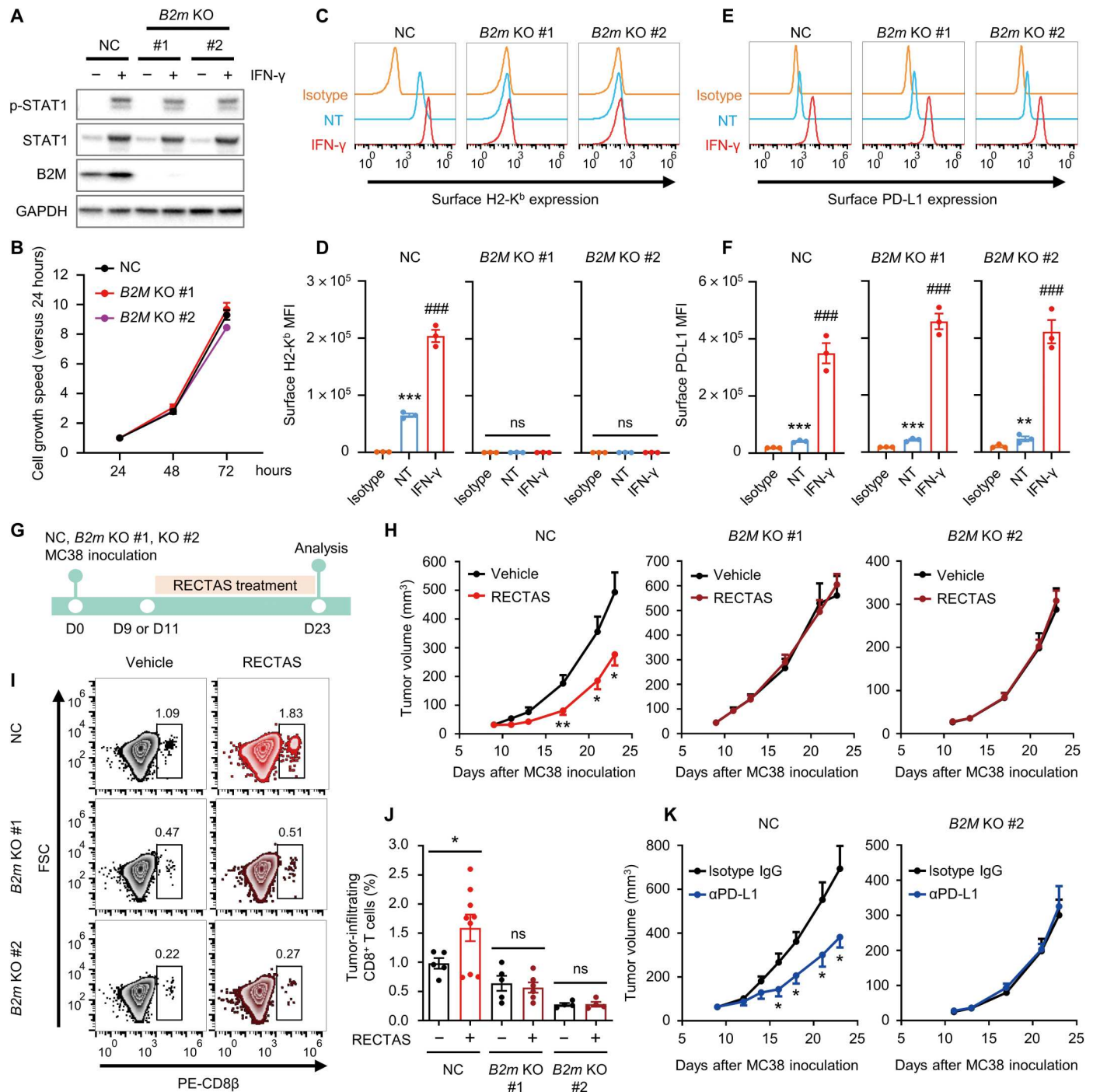
Fig. 2. RECTAS enhances tumor immunogenicity without antigen-independent activation of T cells or autoimmune responses. (A) Experimental procedure of an ex vivo splenocyte assay. Splenocytes were prepared from 8-week-old female C57BL/6N mice and treated with RECTAS for 24 hours. Concanavalin A (ConA) was used as a positive control. (B to E) Frequencies of CD44⁺ and CD69⁺ cells among CD8⁺ T cells in groups with indicated treatments were measured through FCM; representative images (B and C) and quantitative data (D and E) are given (*n* = 3 per group). SSC, side scatter. (F and G) The concentrations of IFN- γ (F) and TNF- α (G) in the supernatant were measured with enzyme-linked immunosorbent assay (ELISA) (*n* = 3 per group). LOD, limit of detection. (H to M) RECTAS (100 mg/kg) or vehicle control (0.5% CMC-Na) was orally (p.o.) administered to 7-week-old female C57BL/6N mice twice daily (b.i.d.) for seven continuous days (I and J) or once daily (q.d.) for 4 weeks (K to M), whereas α PD-L1 antibody or isotype control (isotype IgG) was intraperitoneally (i.p.) injected once weekly. The experimental scheme is indicated in (H). Mice were euthanized on day 7 (*n* = 5 per group) to analyze peripheral white blood cells (WBC) (I) and spleen (J). Body weights (*n* = 6 per group) were monitored weekly (K). CD8 immunohistochemistry (L and M) was performed on day 28 (*n* = 3 per group). Scale bars, 50 μ m. The number of CD8⁺ cells was counted using ImageJ software in three areas of each tissue. All data are shown as means \pm SEM. Experiments were performed at least twice for (B to G) or once for others. ****P* < 0.001 versus vehicle control was determined using one-way ANOVA followed by Bonferroni's multiple comparisons test. ELISA, enzyme-linked immunosorbent assay; WBC, white blood cell.



Downloaded from https://www.science.org at Kyoto University on June 11, 2023

splicing patterns affected by RECTAS in MC38 cells and to identify splice products that could yield potential neoantigens capable of binding to MHC class I (Fig. 4B). Among all splicing events that were affected by RECTAS, we focused on the events that were responsible for creating abnormal coding sequences with nonannotated epitopes not registered in both UniProt and Ensembl to

identify candidate splice-neoantigens. With this approach, we identified 169 RECTAS-induced nonannotated splice events for 130 genes as potential neoantigens, which were further subjected to prioritization based on the prediction scores for the binding affinity of each peptide to MHC class I alleles (H2-K^b and H2-D^b) with NetMHCpan4.1 (25), as well as extents of splice rates and mRNA



Downloaded from <https://www.science.org> at Kyoto University on June 11, 2023

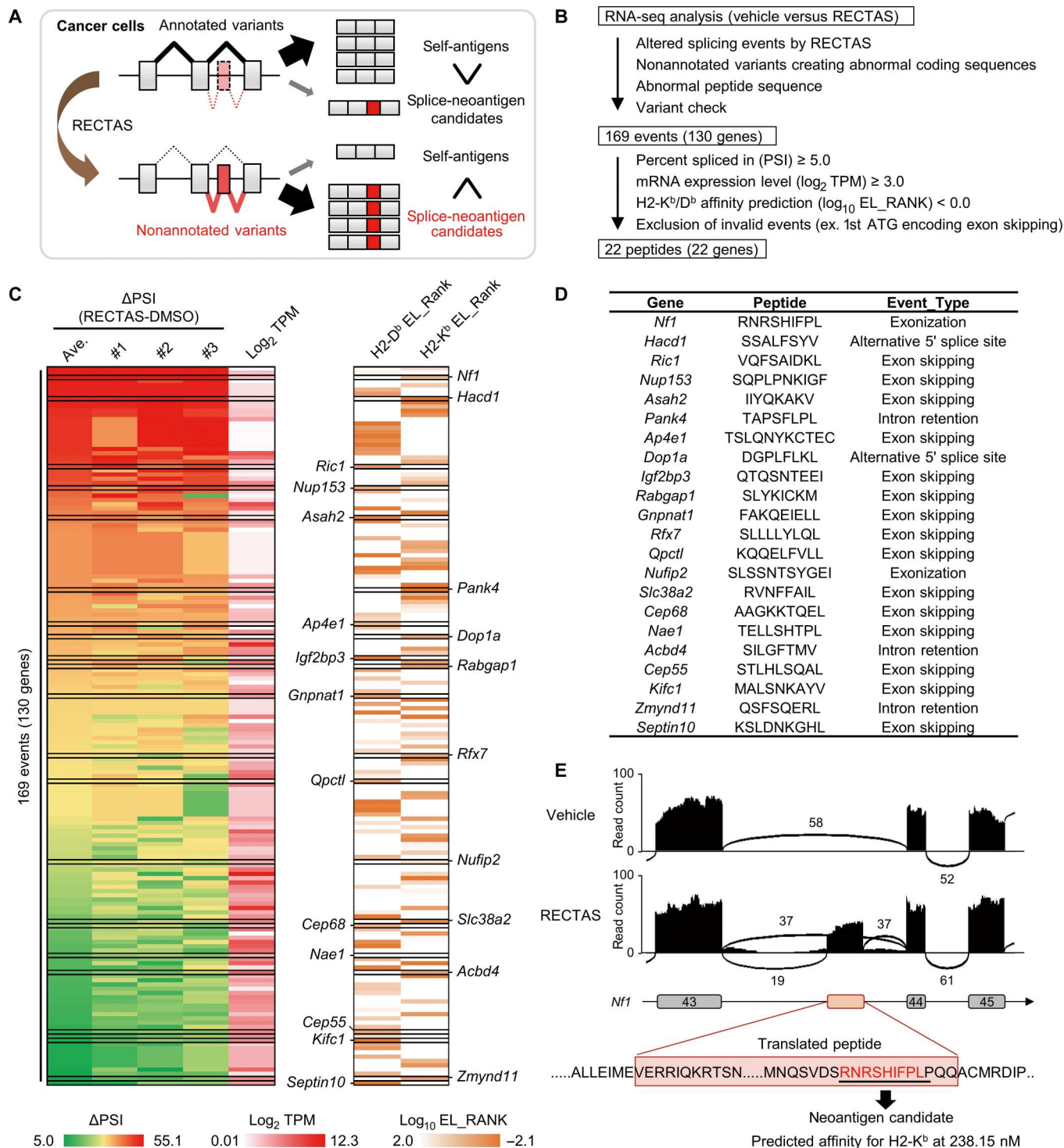


Fig. 4. Identification of RECTAS-inducible splice-neoantigen candidates using RNA-seq analysis. (A) A diagram for RECTAS-mediated induction of splice-neoantigens is shown. (B) A scheme is shown for the screening of RECTAS-induced splice-neoantigen candidates through transcriptome analysis and prediction for MHC class I presentation. RNA-seq was conducted for MC38 cells treated with 10 μ M RECTAS or 0.1% DMSO for 6 hours in three biological replicates each. (C) A heatmap of RECTAS-induced 169 splicing events indicating the difference in values of percent spliced in (Δ PSI; RECTAS – DMSO), \log_2 transcripts per kilobase million (\log_2 TPM; average of RECTAS-treated samples), and \log_{10} eluted ligand rank (\log_{10} EL_RANK) for H2-D^b or H2-K^b. (D) A list of 22 candidate splice-neoantigens is shown. (E) An example of a selected splice-neoantigen candidate is indicated for *Nf1*. The full and curated lists of RECTAS-induced splice-neoantigen candidate data are available in data files S2 and S3, respectively.

expression (Fig. 4C and data file S2). Last, we selected 22 RECTAS-induced splice-neoantigen candidates (8 to 11 amino acids in length) for subsequent evaluation (Fig. 4D and data file S3). An example of this sorted splice alteration is that of *neurofibromin 1* (*Nf1*), in which treatment with RECTAS induced the exonization of 108 base pairs (bp), with the resulting splice product encoding the "RNRSHFPL" candidate neopeptide, previously nonannotated and with a predicted affinity for H2-K^b at 238.15 nM (Fig. 4E). RNA-seq analysis also revealed that treatment with RECTAS had no effect on the mRNA expression of genes encoding conventional neoantigens produced in MC38 cells (fig. S4) (26).

Putative splice-neoantigens induced by RECTAS treatment were validated ex vivo

We next attempted to experimentally validate the immunogenicity of sorted candidates of RECTAS-inducible splice-neoantigens for their binding to MHC class I and activation of CD8⁺ T cells. We synthesized 22 splice-neoantigen candidates and a melanoma antigen peptide, tyrosinase-related protein 2 (TRP2)_{180–188}, as a positive control. Immunocompetent mice were vaccinated twice with the synthesized peptides in the presence of polyinosinic-polycytidylic acid (Poly(I:C)) as an adjuvant. We then prepared splenocytes from vaccinated mice, cocultured them with peptide-pulsed bone marrow-derived dendritic cells (BMDCs) for 24 hours, and evaluated the activation of CD8⁺ T cells using an IFN- γ Enzyme-Linked ImmunoSpot (ELISpot) assay (Fig. 5A). Of the 22 peptides examined, the IFN- γ ELISpot assay identified 6 peptides that were immunogenic and were derived from the altered splicing of *Kifc1*, *Nf1*, *Acbd4*, *Rfx7*, *Qpct1*, and *Nup153* (Fig. 5, B and C). To further validate the binding capability of these six peptides to MHC class I alleles, we assessed the stabilization of surface H2-D^b and H2-K^b using transporter associated with antigen processing 2 (TAP2)-deficient RMA-S cells, in which MHC class I is destabilized because of a lack of peptide presentation (27). In RMA-S cells, H2-D^b- and H2-K^b-orientated affinity of glycoprotein 100 (gp100) and TRP2 antigens were recaptured, and we found that six RECTAS-inducible splice-neoantigens showed affinity to H2-D^b or H2-K^b (Fig. 5D), indicating the presentation of splice-neoantigens by MHC class I. In addition to the RNA-seq analysis, we also validated the induction of these splice-neoantigen-coding transcripts by treatment with RECTAS using reverse transcription polymerase chain reaction (RT-PCR) analysis with neojunction primers in MC38 cells (Fig. 5, E and F). Once the immunogenicity of identified splice-neoantigens by IFN- γ ELISpot assay was confirmed, we then determined whether the identified RECTAS-induced splice-neoantigens are shared across cancer types using the murine Lewis lung carcinoma (LLC), Pan02 pancreatic ductal adenocarcinoma, WEHI3 leukemia, CT26 colorectal adenocarcinoma, EG7 lymphoma, and B16 melanoma cell lines. We found that these splice alterations induced by RECTAS were shared in most of the examined cells (Fig. 5G), suggesting that RECTAS is applicable to a broad spectrum of cancers.

In addition, we also examined the RNA-seq data corresponding to colon, lung, and liver tissues from RECTAS-administered mice to analyze the extent of splicing alterations (fig. S5A). We observed 50 to 60% fewer RECTAS-induced splicing events in the normal tissues as compared to MC38 cells (data file S4). These altered splicing events in normal tissues were likely irrelevant to immunogenicity, considering that overt immune responses were not triggered by

RECTAS in these tissues (Fig. 2, I to M, and fig. S2, B to F) and that none of the validated splice-neoantigen forms were expressed in normal tissues (fig. S5B).

Hexavalent vaccination of splice-neopeptides promotes RECTAS-induced antitumor immune responses

Having confirmed that RECTAS-inducible splice-neoantigens were immunogenic, we then assessed their contribution to antitumor immune responses. For this purpose, we used a coculture assay to ensure tumor killing (Fig. 6A). Splenocytes were prepared from mice vaccinated with either hexavalent splice-neoantigens or an irrelevant TRP2_{180–188} antigen and then further stimulated with BMDCs pulsed with the same antigen(s) in the presence of interleukin-2 (IL-2). Tumor killing activity was quantified on the basis of the frequency of annexin V⁺/carboxyfluorescein diacetate succinimidyl ester-positive (CFSE⁺) cells at 24 hours after coculture with antigen-elicited effector cells and CFSE-prelabeled target cells. Although effector cells from TRP2-immunized mice did not exhibit any response, regardless of peptide loading, hexavalent splice-neoantigen-stimulated effector cells selectively killed MC38 cells presenting six splice-neopeptides (Fig. 6, B and C). Concordantly, this tumor killing activity was absent for the *B2m* KO MC38 cells (Fig. 6D), indicating that this effect was MHC class I-dependent. In addition, the contributions of individual epitopes were also examined through coculture assays for tumor killing, and we observed that most of the epitopes [kinesin family member C1 (KIFC1), neurofibromin 1 (NF1), acyl-CoA binding domain containing 4 (ACBD4), regulatory factor X7 (RFX7), nucleoporin 153 (NUP153)] individually triggered the tumor-killing responses (fig. S6).

We further investigated the tumor-killing responses in the context of cancer cells, which were induced to produce endogenous splice-neoantigens by treating with RECTAS. We found that effector cells isolated from hexavalent-immunized mice exhibited cytotoxic activity against all three cancer cell lines examined: MC38 (Fig. 6E), B16 (Fig. 6F), and LLC (Fig. 6G). All of these lines expressed splice-neoantigens in response to RECTAS treatment (Fig. 5F). In contrast, these effector cells did not show cell lytic activity toward mouse embryonic fibroblasts (MEFs) from B6 mice (Fig. 6H). Expression of splice-neoantigens was low compared with MC38 (fig. S7, A and B), suggesting that MEFs may have avoided CD8⁺ T cell killing owing to a lack of sufficient induction of splice-neoantigens. One of the major phenotypes in antigen-reactive T cells is an acute cell expansion after the recognition of corresponding antigen presented on cancer cells. In the coculture condition with hexavalent peptide-elicited effector cells, we also found increased frequencies of effector cells when MC38 cells were exposed to the hexavalent peptide combination or a subset of those peptides (fig. S8A), as well as to RECTAS (fig. S8B). This effect was also confirmed when purified CD8⁺ T cells were cocultured with MC38 cells (fig. S8, C and D).

Although inducible splicing-derived peptides in cancer cells were previously proposed, their importance in tumor growth in vivo remains uncharacterized (28). Thus, we next investigated whether RECTAS-inducible splice-neopeptide-reactive T cells can suppress tumor growth (Fig. 6I). Hexavalent vaccination on its own resulted in suppressed tumor growth [Poly(I:C) + vehicle versus Poly(I:C)/hexavalent peptide + vehicle, 24.7% suppression on day 23; Fig. 6J and fig. S9A], likely owing to the immunogenicity of

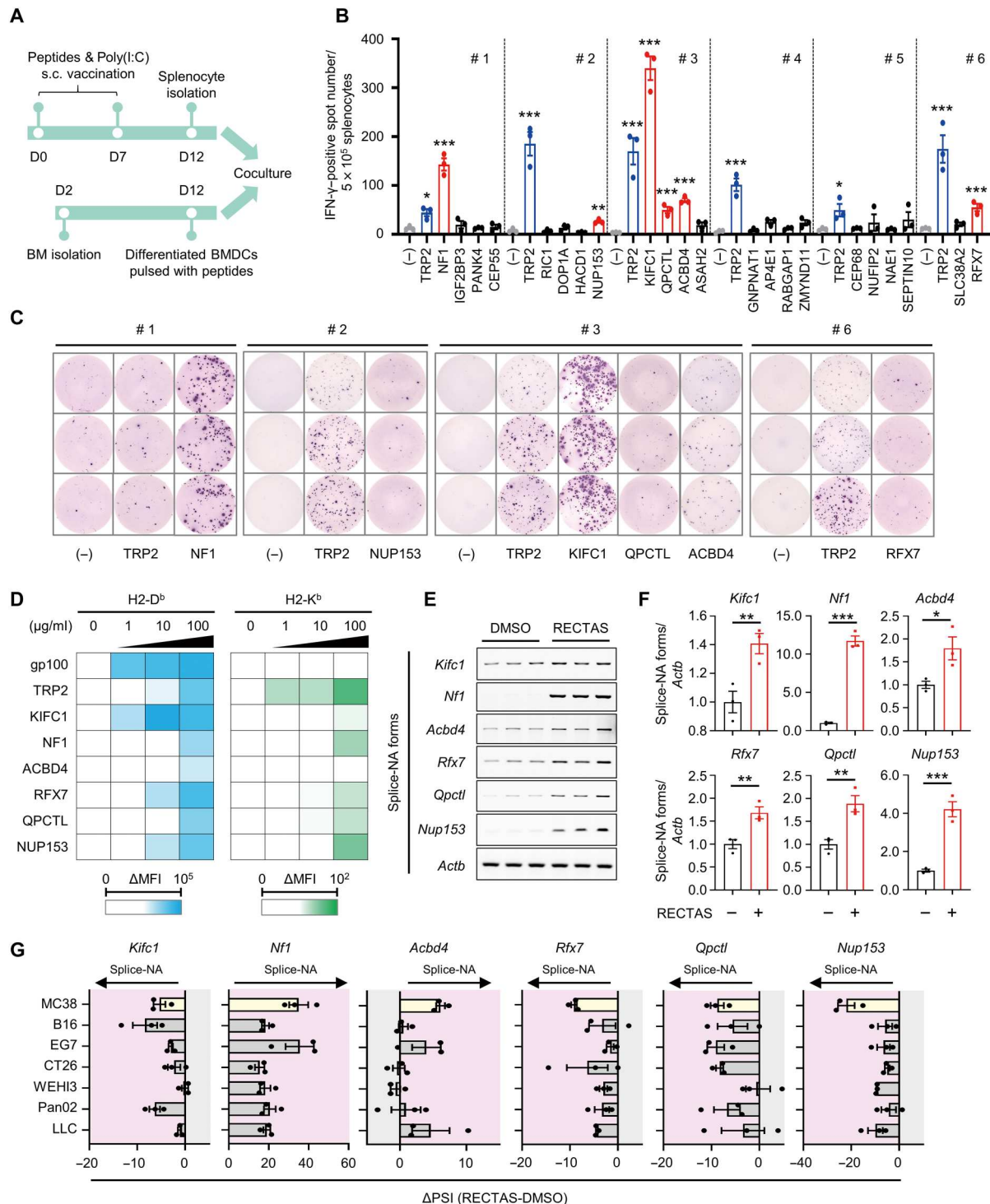


Fig. 5. Ex vivo validation of newly identified splice-neoantigen candidates. (A) A schema for the ELISpot assay is shown. s.c., subcutaneous; BM, bone marrow. (B) IFN- γ ELISpot assay of RECTAS-induced splice-neoantigen candidates ($n = 3$ per peptide). TRP2_{180–188} peptide was used as a positive control. $*P < 0.05$, $**P < 0.01$, and $***P < 0.001$ versus no peptide pulse shown as (-). (C) ELISpot well image of immunogenic peptides examined, as well as the corresponding positive and negative controls. (D) Heatmap of the stabilization of surface H2-D^b and H2-K^b in RMA-S cell assay. gp100 and TRP2 serve as positive controls for H2-D^b and H2-K^b, respectively. Delta-median fluorescent intensity (ΔMFI) was determined by subtracting MFI of control cells (isotype IgG-incubated, without peptide incubation) from MFI of peptide or vehicle-treated cells (anti-H2-D^b-PE or anti-H2-K^b-Alexa Fluor 647-incubated). (E and F) RT-PCR analysis for splice-neoantigen coding forms (splice-NA forms) in MC38 cells treated with 10 μM RECTAS or vehicle control (0.1% DMSO) for 6 hours. Gel images (E) and quantification data (F) are shown ($n = 3$). *Actb* served as a loading control. $*P < 0.05$, $**P < 0.01$, and $***P < 0.001$. (G) Splice-neoantigen producing rates calculated from RNA-seq data ($n = 3$ biological replicates) are indicated as the ΔPSI (RECTAS – DMSO). All data are shown as means \pm SEM. All experiments were performed at least twice. Statistical significance was determined using an unpaired Student's t test for (B) and (F).

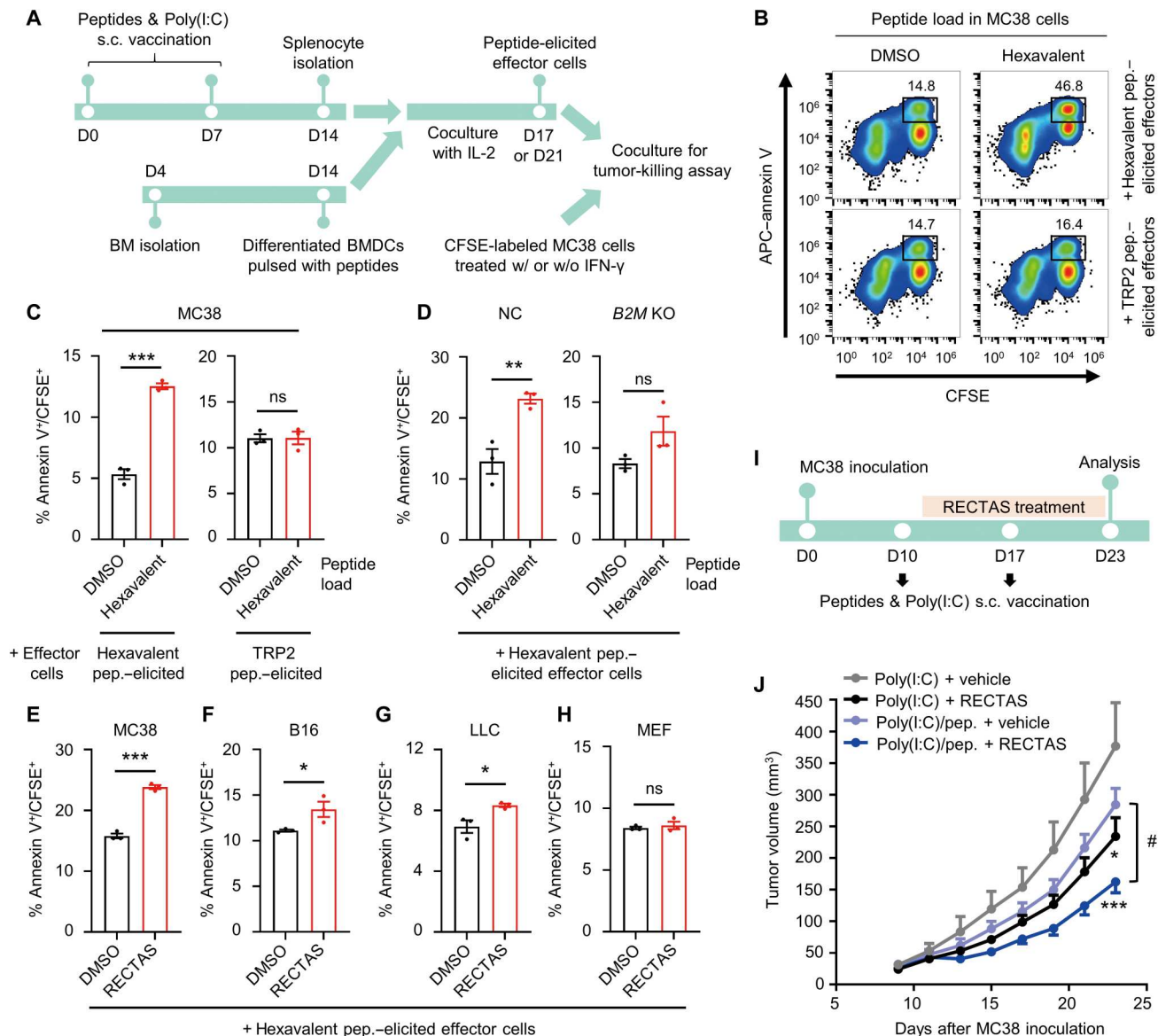


Fig. 6. Hexavalent vaccination of inducible splice-neoepitopes promotes RECTAS-induced antitumor immune responses. (A) A schema for the tumor killing assay is shown. (B and C) Representative flow cytometric images showing tumor killing activity mediated by antigen-elicited effector cells (B) and quantitative data of CFSE⁺/annexin V⁺ frequency (C) are indicated ($n = 3$ per group). APC, allophycocyanin. Hexavalent (Kifc1-, Nf1-, Acbd4-, Rfx7-, Qpctl-, and Nup153-derived) peptides or an irrelevant TRP2₁₈₀₋₁₈₈ peptide was used to elicit antigen-reactive effector cells. CFSE-labeled MC38 cells were stimulated with either 0.1% DMSO or hexavalent peptides for 2 hours and then cocultured with effector cells for 24 hours. Annexin V was used for monitoring early and late apoptotic cell frequencies. $***P < 0.001$. (D) For the NC or B2M KO clone ($n = 3$ per group), CFSE⁺/annexin V⁺ frequencies in the same experimental condition as (C) are shown. $**P < 0.01$. The effector:target ratio was 3:1 for (B to D). (E to H) Effector cells elicited by hexavalent peptide-immunized mice were cocultured with CFSE-labeled target cells in the presence of either 0.1% DMSO or 25 μ M RECTAS for 24 hours. The quantitative data of CFSE⁺/annexin V⁺ ($n = 3$ per group) are shown for MC38 (E), B16 (F), LLC (G), and MEF (H). $*P < 0.05$ and $***P < 0.001$. The effector:target ratio was 5:1 for (E to H). (I) A schema for the vaccination study in MC38 tumor-bearing mice is shown. (J) Tumor volumes of mice are shown ($n = 8$ per group). $*P < 0.05$ and $***P < 0.01$ versus Poly(I:C) + vehicle; # $P < 0.05$ between the indicated groups. All data are shown as means \pm SEM. All experiments were performed at least twice. Statistical significance was determined using an unpaired Student's t test for (C to H) and one-way ANOVA followed by Bonferroni's multiple comparisons test for (J).

basally expressed splice-neoantigens in cancer cells (Fig. 5, E and F). This effect was further enhanced upon coadministration of RECTAS [Poly(I:C) + vehicle versus Poly(I:C)/hexavalent peptide + RECTAS, 57.0% suppression on day 23; Fig. 6] and fig. S9A]. We also evaluated the effect of each splice-neoantigen by individual vaccination with RECTAS and found that there was a 6 to 23%

increase in tumor growth suppression compared with that in non-vaccinated controls (fig. S9B). The tumor-suppressive effects of individual vaccinations were weaker than those of hexavalent vaccinations, wherein the suppression rate was 30.7% (Fig. 6J), indicating that the antitumor immune response was enhanced upon simultaneous vaccination with the six identified neoepitopes.

Given that RECTAS did not induce a complete shrinkage of tumors, we supposed that the underlying mechanism involved the favoring of cancer cells with impaired splice-neoantigen induction by immune selection machinery. However, there was no pronounced change in the expression of splice-neoantigens in response to RECTAS treatment in these cancer cells at the early (day 18) or late (day 42) phases of tumor growth (fig. S10). Thus, we speculated that another mechanism, such as T cell exhaustion (29), might be involved.

DISCUSSION

Alternative pre-mRNA splicing is robustly regulated, and the modulation of SRSF activity affects about 0.3% of total splicing (30). Our previous studies revealed that RECTAS affects only a limited set of splicing events and gene expression in noncancerous cells (16, 21). However, in cancer cells, SRSFs regulate extra sets of splicing events owing to suboptimal splice sites that emerge because of somatic mutations in cis-regulatory elements or alterations in trans-acting splicing factors (31). These cancer-associated alternative splicing events eventually produce irregular splice junctions in cancer cells. Our current study focused on validating whether this process can be promoted with RECTAS administration. Using an immunocompetent MC38 tumor-bearing model, we demonstrated that antitumor effects of RECTAS were mediated by CD8⁺ T cells and MHC class I in cancer cells, which suggested the contribution of splicing-associated neoantigen production. We then succeeded in identifying immunogenic RECTAS-inducible splice-neoepitopes through RNA-seq and subsequent analysis with ex vivo IFN- γ ELISpot assay. The hexavalent vaccination of RECTAS-inducible splice-neoantigens sufficiently elicited endogenous T cell responses for tumor lysis in a coculture assay and led to a suppression of tumor growth in vivo when cancer cells were treated with RECTAS.

Our study also demonstrated that only a small proportion of RECTAS-inducible nonannotated splicing events produce immunogenic epitopes, assuming the rest are not presented on MHC class I or physiologically expressed and subjected to immune tolerance. Given that continuous systemic exposure of normal mice to RECTAS showed no autoimmune responses even in the presence of α PD-L1 antibody, the effect of RECTAS-enhanced tumor immunity explored here is expected to be cancer cell selective. In support of this, RNA-seq analysis revealed that these splice-neoantigens were selectively induced in cancer cells compared with normal tissues. The results of the coculture lysis assay conducted in this study further support the idea of splice-neoantigen-primed tumor lytic response. As cancer cells exhibit splicing patterns distinct from those of nonmalignant cells in terms of both quality and quantity because of mutations accumulated in splicing factors (32) and differential expression of splicing regulators (33), disrupted splicing machineries in cancer cells may make them prone to produce cryptic splice products, as seen for splice-neoantigens reported in the current study. Moreover, we performed a 4-week rat good laboratory practice toxicity study and found that RECTAS had a favorable profile (16). These data together indicated that RECTAS is a safe and promising preclinical candidate for boosting the response to immune checkpoint therapy.

However, our work has some limitations. Although the current study demonstrated the boosted antitumor immune responses by hexavalent peptide immunization, a direct detection of MHC

class I-presented antigens remains to be seen. We attempted mass spectrometry analysis but failed to detect splice-neoantigens, as well as previously reported antigens (26). It is still technically challenging to directly detect a small amount of peptides presented on MHC class I molecule. In addition, we found that RECTAS increased the expression of multiple splice-neoepitopes, but it was not fully validated which splice-neoantigens mainly contributed to tumor immunity. To further validate the contribution of each splice-neoantigen to RECTAS-mediated antitumor effects, it will be important to analyze the clonotype of splice-neoantigen-reactive T cells in tumors after RECTAS treatment. Furthermore, it remains to be determined which types of cancer are susceptible to this therapeutic strategy, although the expansion of neoantigen abundance by leveraging splicing patterns in cancer cells was demonstrated in this study.

In addition to a colorectal cancer, which we mainly used for the in vivo model in the current study, we found that most of the RECTAS-inducible neoepitopes were commonly observed in multiple mouse cancer cell lines across various tumor types, suggesting that a subset of RECTAS-induced pre-mRNA splicing is not only restricted by individual mutations but also may be a common phenomenon in multiple cancer types. Because recognition of tumor neoantigens by host cytotoxic CD8⁺ T cells is crucial for the response to PD-1 blockade, neoantigen vaccination for personalized immunotherapy is a promising approach for potentiating PD-1 blockade cancer therapy (34). However, this approach requires precise identification of the most suitable neoantigen with high immunogenicity and is only applicable to a limited number of patients because neoantigen-producing mutations are mostly specific and not shared among patients (35). Chemical induction of splice-neoantigen expression or a vaccination strategy based on these neoantigens offers a promising approach for overcoming these issues by enhancing the production of multiple immunogenic splice-neoantigens across cancer types. A consensus from meta-analyses of PD-1 blockade is that a favorable clinical outcome is anticipated in cohorts with a higher tumor mutation burden (TMB) compared with that in cohorts with a lower TMB (9, 36, 37). Nonetheless, a recent survey of TMB for more than 100,000 specimens across cancer types indicated that in most types of cancer, the median TMB is lower than 10 mutations/Mb. This is a frequently applied threshold for a low TMB and is concordant with limited clinical benefits of PD-1 blockade (38). In this respect, the RECTAS-induced generation of splice-neoantigens (fig. S11) would not only enhance the clinical response to PD-1 blockade for patients with high TMB but also sensitize those with low TMB. Overall, the current study identifies chemically inducible neoantigens applicable for cancer vaccination and provides a new concept of splice-leveraging cancer immunotherapy with ICIs.

MATERIALS AND METHODS

Study design

The objective of this study was to validate the concept that synthetic pre-mRNA splicing modifiers boosted antitumor immune responses through inducible splicing-associated neoantigens. First, we conducted tumor-bearing animal experiments in immunocompetent mice to confirm whether the splicing modifier RECTAS suppressed tumor growth by boosting antitumor immunity. Having confirmed that RECTAS treatment led to a reduction in tumor growth in a

CD8⁺ T cell and tumor MHC I–dependent manner and also that RECTAS potentiated PD-1 blockade efficacy, we next attempted to explore the potential neoantigens induced by RECTAS. To address this, RNA-seq was performed to extract nonannotated splice variants induced or enhanced by RECTAS, creating abnormal peptides translated from these variants. Among extracted neoantigen candidates, we screened and identified immunogenic peptides using IFN- γ ELISpot assays. Subsequently, in vivo vaccination studies revealed that immunization of chemically inducible splice-neoantigens elicited endogenous T cell responses for tumor lysis under coculture conditions and led to a suppression of tumor growth when cancer cells were sensitized with RECTAS. Determination of sample sizes for cell and animal experiments was based on previous reports. Animals were randomly divided into experimental groups according to body weight or tumor volume. All experiments were unblinded. The number of replicates for each experiment is presented in the figure legends.

Animals

All animal procedures used in this study were conducted according to the guidelines of the Institutional Animal Care and Use Committee of Graduate School of Medicine, Kyoto University. Female C57BL/6N mice aged 6 or 7 weeks were purchased from Charles River Laboratories Japan. Animals were maintained under specific pathogen-free conditions.

Cell lines

Mouse cancer cell lines were obtained as described previously (39). Cells were cultured in RPMI 1640 or Dulbecco's modified Eagle medium (DMEM; Nacalai Tesque) supplemented with 10% (w/w) heat-inactivated fetal bovine serum (FBS; Thermo Fisher Scientific) and penicillin/streptomycin (P/S; 100 U/ml; Thermo Fisher Scientific) at 37°C under 5% CO₂ conditions. RMA-S cells, the TAP2-deficient lymphoma cells lacking peptide loading on cell surface H2-K^b and H2-D^b with stable expression of human B2M, were established previously (27). The RMA-S cells were cultured in RPMI 1640 with 10% FBS and P/S (100 U/ml) at 37°C under 5% CO₂ conditions.

Preparation of primary MEFs

MEFs were prepared from pregnant C57BL/6N mice. Each 13- to 15-day-old embryo was dissected from the uterus and washed with phosphate-buffered saline (PBS). After the removal of the head, tail, limbs, and blood-enriched organs, the trimmed embryo was washed with PBS and minced. After trypsinization at 37°C for 10 min followed by inactivation of trypsin by addition of FBS, MEFs were separated by filtration through a 70- μ m cell strainer. The established MEFs were maintained in DMEM containing a high concentration of glucose, 10% FBS, 50 μ M 2-mercaptoethanol (2-ME), and P/S (100 U/ml) at 37°C under 5% CO₂ conditions.

Cell viability and cytotoxicity assay

Cells were seeded in 96-well plates in triplicate and incubated overnight. The next day, cells were treated with the test substances or vehicle control [0.1% dimethyl sulfoxide (DMSO)] and then further incubated for the indicated time. Cell viability and cytotoxicity were respectively measured using a Cell Counting Kit-8 (CCK-8) kit and Cytotoxicity lactate dehydrogenase (LDH) Assay Kit-WST (Dojindo) according to the manufacturer's instructions.

Absorbance was measured with an ARVO X5 multimode plate reader (PerkinElmer).

CRISPR-Cas9-mediated gene editing

For the establishment of *B2m*-KO clones, a nontargeting negative control single-guide RNA (sgRNA) (nontargeting control, 5'-GTA TTA CTG ATA TTG GTG GG-3') and sgRNAs targeting *B2m* (*B2m* #1, 5'-TTG AAT TTG AGG GGT TTC TG-3' and *B2m* #2, 5'-TCA CGC CAC CCA CCG GAG AA-3') were cloned into the pSpCas9(BB)-2A-Puro (PX459) V2.0 plasmid (Addgene, no. 62988) as described previously (40). MC38 cells were transfected using Lipofectamine 2000 (Thermo Fisher Scientific) per the manufacturer's instructions. After incubation for 24 hours, cells were reseeded in 10-cm dishes with 5-, 25-, or 250-fold dilution and treated with puromycin (4 μ g/ml; InvivoGen). Ten days later, colonies expanded from each clone were isolated with trypsin–0.25% EDTA (Thermo Fisher Scientific) using cloning cylinders (Sigma-Aldrich). Isolated clones were screened using FCM and Western blotting to confirm the loss of H2-K^b and B2M expression, respectively. Oligonucleotide sequences are listed in data file S5.

Tumor-bearing model

MC38 cells (5×10^5) were intradermally injected in the right flank of 7- or 8-week-old female C57BL/6N mice (day 0). Mice were randomly divided into experimental groups when the tumor volume reached 30 to 50 mm³ (around day 7 to 11). Antibody administration or peptide vaccination was initiated on the day of grouping, and compound treatment was administered from the following day. Mice were intraperitoneally injected once a week with 35 μ g of α PD-L1 monoclonal antibody (clone 1-111A.4 generated in the laboratory of T.H.), 100 μ g of α CD8 α monoclonal antibody (clone 53-6.7; Bio X Cell), or rat IgG2a, κ (clone 2A3; Bio X Cell) as an isotype control. For peptide vaccination experiments, peptides were synthesized by GenScript Japan with >90% purity and dissolved in DMSO at a concentration of 10 mg/ml until use. Peptides (100 μ g each of KIFC1 [MALSNKAYV], NF1 [RNRSHIFPL], ACBD4 [SILGFTMV], RFX7 [SLLLLYLQL], QPCTL [KQQLFVLL], and NUP153 [SQPLNKIGF]) mixed with 50 μ g of Poly(I:C) (R&D Systems) were subcutaneously injected at the same intervals as antibody injection. Compound or vehicle control (0.1% DMSO) was intratumorally injected once daily. Tumor sizes were measured using a digimatic caliper (Mitutoyo Corporation) at indicated days, and tumor volume was calculated using the formula for a typical ellipsoid [$\pi \times (\text{length} \times \text{breadth} \times \text{height})/6$]. Experiments were performed with $n \geq 5$ in principle or $n \geq 10$ of mice per group for multigroup (group ≥ 3) studies, due to the variation in individual tumor growth.

Single-cell preparation for subsequent analysis

For splenocyte analysis, spleens were harvested from mice and disrupted with the plunger of a syringe on a 70- μ m cell strainer to prepare a single-cell suspension. After washing with PBS, splenocyte suspensions were treated with ACK lysis buffer (Thermo Fisher Scientific) at room temperature for 5 min to lyse the erythrocytes. Then, cells were resuspended with RPMI 1640 + 10% FBS + P/S (100 U/ml) and seeded in a 96-well plate (1×10^6 cells per well) for ex vivo splenocyte activation assay. For tumor-infiltrating lymphocyte analysis, tumors were harvested from mice on indicated days after inoculation. Tumors were then minced into 2- to 3-mm pieces with scissors and

subsequently digested with a tumor dissociation kit using a gentle-MACS Dissociator (Miltenyi Biotec). Regarding the FCM analysis, dissociated cells from spleens and tumors were incubated with FCM buffer [0.5% bovine serum albumin (BSA) and 2 mM EDTA in PBS] containing anti-mouse CD16/CD32 antibody for Fc Block (clone 2.4G2; BD Biosciences) for 5 min on ice before staining with primary antibodies.

Flow cytometry

Cells were suspended in FCM buffer and stained for 30 min on ice with the following monoclonal antibodies against the indicated antigens: CD3 ϵ -Alexa Fluor 488 (clone 145-2C11, 2 μ g/ml), CD4-Alexa Fluor 647 (clone RM4-5, 2 μ g/ml), and CD11b-Alexa Fluor 647 (clone M1/70, 2 μ g/ml) from BD Biosciences; CD8 β -phycoerythrin (PE; clone YTS156.7.7, 2 μ g/ml), PD-L1-PE (clone 10F.9G2, 2 μ g/ml), H2-K^b-Alexa Fluor 647 (clone AF6-88.5, 5 μ g/ml), CD11c-Alexa Fluor 647 (clone N418, 5 μ g/ml), F4/80-Alexa Fluor 488 (clone BM8, 5 μ g/ml), CD44-PE/Cy7 (clone IM7, 2 μ g/ml), and CD69-PE/Cy7 (clone H1.2F3, 2 μ g/ml) from BioLegend. Unless otherwise specified, all FCM experiments were performed on an Accuri C6 Plus flow cytometer (BD Biosciences) and analyzed using FlowJo software version 10.7.2 (FlowJo LLC).

Tumor cell isolation and analysis

Tumor cells were isolated from intradermally transplanted tumors on days 18 and 42 after inoculation with negative selection using the tumor dissociation kit followed by tumor cell isolation kit (Miltenyi Biotec) per the manufacturer's instructions. Isolated tumor cells were cultured on dishes in RPMI 1640 with 10% FBS and P/S (100 U/ml) overnight at 37°C under 5% CO₂ conditions. The next day, cells were treated either with RECTAS or 0.1% DMSO for 6 or 24 hours, and then total RNA was extracted from treated cells for RT-PCR analysis.

ELISpot assay

Eight-week-old female C57BL/6N mice were subcutaneously injected with 100 μ g of synthesized peptides (GenScript Japan) and 50 μ g of Poly(I:C) formulated in PBS (\leq 5 peptides per mouse) on days 0 and 7. H2-K^b-restricted TRP2_{180–188} peptide [SVYDFVWL] (MBL International) was used as a positive control. Mice were euthanized 12 days after the initial injection, and splenocytes were isolated. As stimulators, BMDCs were generated as described previously (41) with some modifications. Briefly, bone marrow cells were isolated from femurs of 8-week-old female C57BL/6N mice through centrifugation on day 2. Cells were passed through a 70- μ m cell strainer and seeded in 10-cm petri dishes with RPMI 1640 containing 10% FBS, P/S (100 U/ml), 2 mM L-glutamine, 50 μ M 2-ME, and granulocyte-macrophage colony-stimulating factor (20 ng/ml; PeproTech). Culture was maintained by replacing half of the medium every 2 or 3 days. On day 12, most of the nonadherent cells had acquired typical dendritic morphology, and these cells were pulsed with peptides (2 μ g/ml) for 2 hours at 37°C. ELISpot assay was performed using Mouse IFN- γ ELISpot BASIC kit (Mabtech AB) per the manufacturer's instructions. Freshly isolated splenocytes (5×10^5 cells) were cocultured with peptide-pulsed BMDCs (4×10^4 cells) overnight at 37°C under 5% CO₂ conditions in an ELISpot polyvinylidene difluoride (PVDF) white plate coated with anti-IFN- γ antibody (clone AN18). Then, IFN- γ secretion was detected using capture antibody (clone R4-6A2) and 5-brom-4-

chlor-3-indolylphosphat/nitro blue tetrazolium-plus substrate. After leaving the plate to dry, the spot number was counted using a dissection microscope. Spot images were acquired using an ImmunoSpot S6 Ultimate analyzer (Cellular Technology Limited).

MHC class I stability assay with RMA-S cells

RMA-S cells were cultured at 26°C under 5% CO₂ overnight (at least 14 hours) to allow expression of empty MHC class I without peptide presentation. The RMA-S cells were then incubated with peptides for H2-D^b-restricted gp100_{25–33} [KVPRNQDWL] (MBL International) and H2-K^b-restricted TRP2_{180–188}, KIFC1, NF1, ACBD4, RFX7, QPCTL, or NUP153 at 0, 1, 10, or 100 μ g/ml with 1% DMSO in culture media for 1 hour at 26°C under 5% CO₂ conditions, to induce peptide-loading on MHC class I, followed by incubation at 37°C under 5% CO₂ for 3 hours to destabilize MHC class I without peptide presentation. Cells were then washed three times with FCM buffer at 37°C and incubated with Fc Block for 5 min at 4°C. Cells were then incubated with anti-H2-K^b-Alexa Fluor 647 (clone AF6-88.5, 5 μ g/ml; BioLegend) or isotype mouse IgG2a-Alexa Fluor 647 control (clone MOPC-173, 5 μ g/ml; BioLegend), and anti-H2-D^b-PE (clone KH95, 2 μ g/ml; BioLegend) or isotype mouse IgG2b-PE control (clone 3D12, 2 μ g/ml; MBL International), for 1 hour at 4°C, followed by washing four times and analysis using the Attune NxT Acoustic Focusing Cytometer (Thermo Fisher Scientific). FCM data were analyzed using FlowJo software version 10.8.1, and individual Δ median fluorescent intensities (MFIs) were determined by subtracting MFI from isotype IgG controls (mouse IgG2a-Alexa Fluor 647 and mouse IgG2b-PE) without peptide loading from each MFI from anti-H2-K^b-Alexa Fluor 647 and anti-H2-D^b-PE. Resulting Δ MFI was plotted for relative quantification of promoted MHC class I stability by peptide loading.

Coculture assay for the measurement of tumor killing activity

Splenocytes were prepared from peptide-vaccinated mice with Poly(I:C) on day 14, as described in the section of "ELISpot assay." To further elicit antigen-specific CD8⁺ T cells, freshly isolated splenocytes were cocultured with peptide-pulsed BMDCs in the presence of IL-2 (10 ng/ml; PeproTech) for another 3 or 7 days. Culture was maintained by replacing half of the medium every 2 or 3 days. Splenocytes stimulated with BMDCs, as effector cells, were then cocultured with target cells at an effector:target ratio of 3:1 or 5:1 for 24 hours to examine their lytic activity. For the preparation of target cells, in the previous day of coculture with effector cells, cells were labeled with 2 μ M CFSE (Dojindo) for 10 min, and the labeling reaction was stopped by an additional 10 min of incubation with FBS. After washing with medium twice, cells were cultured overnight in the presence of IFN- γ (10 ng/ml). The next day, target cells were pulsed with peptide(s) (10 ng/ml) for 2 hours before coculture or treated with RECTAS in the presence of effector cells. After coculture for 24 hours, cells were stained with annexin V (BioLegend) in annexin V binding buffer (MBL) for 15 min and subjected to FCM analysis. Effector cell-mediated killing activity was calculated from the frequencies of annexin V⁺/CFSE⁺.

Western blotting

Cells were lysed with SDS sample buffer [100 mM tris-HCl (pH 6.8), 4% SDS, and 10% glycerol] and sonicated. Protein

concentrations were determined using a bicinchoninic acid protein assay (Thermo Fisher Scientific) according to the manufacturer's instructions. Then, 2-ME and bromophenol blue were added to the proteins to a final concentration of 5 and 0.025%, respectively, and boiled for 5 min. Equal amounts of protein were subjected to SDS-polyacrylamide gel electrophoresis and transferred onto PVDF membranes. The membranes were blocked with Blocking One solution (Nacalai Tesque) for 1 hour at room temperature and then probed with appropriate primary antibodies overnight at 4°C in Can Get Signal Solution 1 (TOYOBO). The next day, the membranes were washed with tris-buffered saline [TBS; 50 mM tris-HCl (pH 7.4) and 150 mM NaCl] containing 0.05% Tween 20 (TBS-T) and incubated with the horseradish peroxidase (HRP)-conjugated goat anti-mouse IgG-F(ab')₂ (1:10,000; Abcam) or HRP-conjugated donkey anti-rabbit IgG-F(ab')₂ (1:20,000; Sigma-Aldrich) in TBS-T for 1 hour at room temperature. After washing with TBS-T, the membranes were incubated with Chemi-Lumi One Super (Nacalai Tesque). The specific proteins were visualized using a ChemiDoc MP Imaging System (Bio-Rad Laboratories), and the data were analyzed using ImageJ software version 1.52. Primary antibodies against the following proteins were used: phospho-STAT1 (clone 58D6, 1:1000), STAT3 (clone 124H6, 1:1000), and glyceraldehyde-3-phosphate dehydrogenase (GAPDH; clone D16H11, 1:5000) from Cell Signaling Technology; STAT1 (clone EPYR2154, 1:500) and phosphor-STAT3 (clone EP2147Y, 1:500) from GeneTex; and B2M (clone EP2978Y, 1:500) from Abcam.

Reverse transcription polymerase chain reaction

Total RNA was extracted from cells using an RNeasy Mini Kit (QIAGEN), according to the manufacturer's protocol, and subjected to reverse transcription using a High-Capacity cDNA Reverse Transcription Kit (Applied Biosystems). Genes were amplified with KOD One DNA polymerase (TOYOBO) and target-specific primer sets. RT-PCR products were separated using electrophoresis. Ethidium bromide-stained images were captured using a ChemiDoc MP Imaging System, and the data were analyzed using ImageJ software. The following primers were used: 5'-TTC CTG TGA GAA AGA GGT GGA G-3' (oSM150) and 5'-CAC AAA CAT AAG CCT TAT TGC TCA G-3' (oSM165) for *Kif1*, 5'-CAC TTT AGT GAA GAG ACC AAG CAA G-3' (oSM172) and 5'-TCA TAC ATG CTT GTT GTG GCA GAG-3' (oSM174) for *Nfl*, 5'-CAT GGG TAC CGA GAA GGA AGA G-3' (oSM156) and 5'-TCC AAT GGG GTC CCA GAA C-3' (oSM157) for *Acbd4*, 5'-AAA CTG GAG ATG GGG ACT TA-3' (oSM168) and 5'-TGA GGA TTC TCC TGG CAA TG-3' (oSM155) for *Rfx7*, 5'-CCA AGT GAG AAA GTT CCT GGA G-3' (oSM152) and 5'-GAG GAC AAA GAG CTC CTG CTG-3' (oSM169) for *Qpctl*, 5'-CCA GAG AAT GAG GAA GTG GAA G-3' (oSM163) and 5'-GTA AAT CCA ATC TTG TTT GG-3' (oSM166) for *Nup153*, and 5'-TCT TTG CAG CTC CTT CGT TG-3' (oSM158) and 5'-GGC CTC GTC ACC CAC ATA G-3' (oSM159) for *Actb*. *Actb* was used as a loading control. Oligonucleotide sequences are listed in data file S5.

RNA-seq and identification of splice-neoantigen candidate

Total RNA was extracted from mouse cancer cell lines treated with RECTAS (10 μM) or vehicle control (0.1% DMSO) for 6 hours. RNA-seq libraries were prepared using a TruSeq Stranded mRNA Library Kit (Illumina) and used for paired-end sequencing on the

Illumina NovaSeq 6000 platform. RNA-seq data were mapped to the GRCh38 (mm10) genome sequence using HISAT2 program version 2.2.0 with the "--rna-strandness RF" option (42). Splice-junction information available from Ensembl gene annotation version 100 was used in this process (43). Mapped results were discarded when either of the paired reads was not mapped to the genome or the relationships of mapping positions were abnormal. For splicing analysis, rMATS program version 4.1.0 was used (44). For the reference transcript models used in the rMATS analysis, a set of new transcripts based on RNA-seq data was constructed using Cufflinks program version 2.2.1 (45). Because the rMATS program skips soft-clipped reads and reads having indels in their alignment, bam files were modified to replace soft clipping and indel information as not changing the splice position information, following the method described previously (46). After rMATS analysis, altered spliced events were extracted according to the following criteria: false discovery rate < 0.01, delta PSI (dPSI) ≥ 5.0, and average number of spliced reads ≥ 15 in either of the samples. Altered spliced regions were compared with Ensembl gene annotations for describing the amino acid sequence encoded in these regions. Amino acid sequences not observed in the original peptide database were searched and stored with seven amino acids margins from known sequences. For predicting affinities of splicing-derived peptides to MHC class I (H2-K^b and H2-D^b), NetMHCpan version 4.1 with option "-l 8,9,10,11" was performed (25). For differentially expressed gene (DEG) analysis, transcripts per million (TPM) values and raw reads counts were calculated with RSEM program version 1.2.31 (47). Then, DESeq2 program version 1.8.2 (48) was used to find DEGs fulfilling the following criteria: adjusted *P* < 0.05, fold change ≥ 1.3 or ≤ 1/1.3, average TPM ≥ 1, and average raw read counts ≥ 32 in either of the samples.

Safety assessment in mice with RECTAS treatment

For the assessment of acute response, 7-week-old female C57BL/6N mice were orally administered RECTAS (100 mg/kg) or vehicle control [0.5% *O*-carboxymethylcellulose (CMC)-Na] twice daily for seven consecutive days. In addition, 35 μg of αPD-L1 or isotype control was injected intraperitoneally on day 0. Seven days after initial administration, mice were anesthetized with isoflurane (Pfizer Japan Inc.), and spleen was harvested after collecting peripheral blood from the inferior vena cava with anticoagulant-treated tube. Spleen and peripheral blood samples were treated with ACK lysis buffer followed by anti-mouse CD16/CD32 antibody for Fc Block and subjected to subsequent FCM analysis. For the chronic treatment study, experiments were performed by Nihon Bioresearch Inc. Seven-week-old female C57BL/6N mice were orally administered RECTAS (100 mg/kg) or vehicle control (0.5% CMC-Na) once daily for 4 weeks. Either 35 μg of αPD-L1 or isotype control was injected intraperitoneally once weekly. Animal monitoring was performed daily for general condition and weekly for body weight and food consumption. Four weeks after initial administration, mice were anesthetized with isoflurane, and peripheral blood was collected for the measurement of biochemical parameters. Tissues (colon, skin, and lung) were also harvested and fixed with 10% neutral-buffered formalin for histological analysis.

Histological analysis

Fixed tissues were embedded with paraffin. Blocks were sectioned and stained with hematoxylin and eosin or anti-CD8 antibody

(clone EPR21769, Abcam). Regarding the analysis for CD8 immunocytochemistry, endogenous peroxidase activity was blocked with 0.3% H₂O₂ in methyl alcohol for 30 min after deparaffinization and antigen retrieval by citrate buffer for 5 min at 121°C. The glass slides were washed in PBS (5 min × 6 times) and mounted with 1% normal serum in PBS for 30 min. Subsequently, anti-CD8 antibody (1:2000) was applied overnight at 4°C. Then, they were incubated with biotinylated second antibody (1:300) in PBS for 40 min, followed by washes in PBS (5 min × 6 times). Avidin-biotin-peroxidase complex (Elite ABC; Vector Laboratories) in BSA (1:100) was applied for 50 min. After washing in PBS (5 min × 6 times), coloring reaction was carried out with 3,3-diaminobenzidine, and nuclei were counterstained with hematoxylin. Images were acquired using a BZ-X710 microscope (Keyence), and the number of CD8⁺ cells was counted using the ImageJ software with “Multi-point” tool.

Statistical analysis

All raw, individual-level data are presented in data file S6. Comparisons between two groups were performed using an unpaired Student's *t* test. For multiple comparisons, data were analyzed using one-way analysis of variance (ANOVA) followed by Bonferroni's multiple comparisons test. Statistical analyses were performed using GraphPad Prism version 9.2.0 (GraphPad Software). In all analyses, *P* values < 0.05 were considered to indicate statistical significance.

Supplementary Materials

This PDF file includes:

Figs. S1 to S11

Other Supplementary Material for this manuscript includes the following:

MDAR Reproducibility Checklist

Data files S1 to S6

[View/request a protocol for this paper from Bio-protocol.](#)

REFERENCES AND NOTES

1. T. N. Schumacher, R. D. Schreiber, Neoantigens in cancer immunotherapy. *Science* **348**, 69–74 (2015).
2. C. Tomasetti, L. Li, B. Vogelstein, Stem cell divisions, somatic mutations, cancer etiology, and cancer prevention. *Science* **355**, 1330–1334 (2017).
3. Y. Iwai, M. Ishida, Y. Tanaka, T. Okazaki, T. Honjo, N. Minato, Involvement of PD-L1 on tumor cells in the escape from host immune system and tumor immunotherapy by PD-L1 blockade. *Proc. Natl. Acad. Sci. U.S.A.* **99**, 12293–12297 (2002).
4. T. Okazaki, S. Chikuma, Y. Iwai, S. Fagarasan, T. Honjo, A rheostat for immune responses: The unique properties of PD-1 and their advantages for clinical application. *Nat. Immunol.* **14**, 1212–1218 (2013).
5. S. L. Topalian, C. G. Drake, D. M. Pardoll, Immune checkpoint blockade: A common denominator approach to cancer therapy. *Cancer Cell* **27**, 450–461 (2015).
6. N. Borcherding, R. Kolb, J. Gullicksrud, P. Vikas, Y. Zhu, W. Zhang, Keeping tumors in check: A mechanistic review of clinical response and resistance to immune checkpoint blockade in cancer. *J. Mol. Biol.* **430**, 2014–2029 (2018).
7. K. Chamoto, R. Hatae, T. Honjo, Current issues and perspectives in PD-1 blockade cancer immunotherapy. *Int. J. Clin. Oncol.* **25**, 790–800 (2020).
8. R. G. Gupta, F. Li, J. Roszik, G. Lizée, Exploiting tumor neoantigens to target cancer evolution: Current challenges and promising therapeutic approaches. *Cancer Discov.* **11**, 1024–1039 (2021).
9. M. Yarchoan, A. Hopkins, E. M. Jaffee, Tumor mutational burden and response rate to PD-1 inhibition. *N. Engl. J. Med.* **377**, 2500–2501 (2017).
10. A. Kahles, K. Van Lehmann, N. C. Toussaint, M. Hüser, S. G. Stark, T. Sachsenberg, O. Stegle, O. Kohlbacher, C. Sander; Cancer Genome Atlas Research Network, G. Rättsch,

Comprehensive analysis of alternative splicing across tumors from 8,705 patients. *Cancer Cell* **34**, 211–224.e6 (2018).

11. R. G. Jayasinghe, S. Cao, Q. Gao, M. C. Wendl, N. S. Vo, S. M. Reynolds, Y. Zhao, H. Climent-González, S. Chai, F. Wang, R. Varghese, M. Huang, W.-W. Liang, M. A. Wyczalkowski, S. Sengupta, Z. Li, S. H. Payne, D. Fenyó, J. H. Miner, M. J. Walter; Cancer Genome Atlas Research Network, B. Vincent, E. Eyras, K. Chen, I. Shmulevich, F. Chen, L. Ding, Systematic analysis of splice-site-creating mutations in cancer. *Cell Rep.* **23**, 270–281.e3 (2018).
12. A. C. Smart, C. A. Margolis, H. Pimentel, M. X. He, D. Miao, D. Adeegbe, T. Fugmann, K. K. Wong, E. M. Van Allen, Intron retention is a source of neoepitopes in cancer. *Nat. Biotechnol.* **36**, 1056–1058 (2018).
13. M. Oka, L. Xu, T. Suzuki, T. Yoshikawa, H. Sakamoto, H. Uemura, A. C. Yoshizawa, Y. Suzuki, T. Nakatsura, Y. Ishihama, A. Suzuki, M. Seki, Aberrant splicing isoforms detected by full-length transcriptome sequencing as transcripts of potential neoantigens in non-small cell lung cancer. *Genome Biol.* **22**, 9 (2021).
14. J. Bigot, A. I. Lalanne, F. Lucibello, P. Gueguen, A. Houy, S. Dayot, O. Ganier, J. Gilet, J. Tosello, F. Nemati, G. Pierron, J. J. Waterfall, R. Barnhill, S. Gardrat, S. Piperno-Neumann, T. Popova, V. Masson, D. Loew, P. Mariani, N. Cassoux, S. Amigorena, M. Rodrigues, S. Alsafadi, M. Stern, O. Lantz, Splicing patterns in *SF3B1*-mutated uveal melanoma generate shared immunogenic tumor-specific neoepitopes. *Cancer Discov.* **11**, 1938–1951 (2021).
15. M. Muraki, B. Ohkawara, T. Hosoya, H. Onogi, J. Koizumi, T. Koizumi, K. Sumi, J. I. Yomoda, M. V. Murray, H. Kimura, K. Furuichi, H. Shibuya, A. R. Krainer, M. Suzuki, M. Hagiwara, Manipulation of alternative splicing by a newly developed inhibitor of Clks. *J. Biol. Chem.* **279**, 24246–24254 (2004).
16. M. Ajiro, T. Awaya, Y. J. Kim, K. Iida, M. Denawa, N. Tanaka, R. Kurosawa, S. Matsushima, S. Shibata, T. Sakamoto, L. Studer, A. R. Krainer, M. Hagiwara, Therapeutic manipulation of *IKBKAP* mis-splicing with a small molecule to cure familial dysautonomia. *Nat. Commun.* **12**, 4507 (2021).
17. A. Nishida, N. Kataoka, Y. Takeshima, M. Yagi, H. Awano, M. Ota, K. Itoh, M. Hagiwara, M. Matsu, Chemical treatment enhances skipping of a mutated exon in the dystrophin gene. *Nat. Commun.* **2**, 308 (2011).
18. B. Boisson, Y. Honda, M. Ajiro, J. Bustamante, M. Bendavid, A. R. Gennery, Y. Kawasaki, J. Ichishima, M. Osawa, H. Nihira, T. Shiba, T. Tanaka, M. Chrabieh, B. Bigio, H. Hur, Y. Itan, Y. Liang, S. Okada, K. Izawa, R. Nishikomori, O. Ohara, T. Heike, L. Abel, A. Puel, M. K. Saito, J. L. Casanova, M. Hagiwara, T. Yasumi, Rescue of recurrent deep intronic mutation underlying cell type-dependent quantitative NEMO deficiency. *J. Clin. Invest.* **129**, 583–597 (2019).
19. S. Shibata, M. Ajiro, M. Hagiwara, Mechanism-based personalized medicine for cystic fibrosis by suppressing pseudo exon inclusion. *Cell Chem. Biol.* **27**, 1472–1482.e6 (2020).
20. I. Boussaad, C. D. Obermaier, Z. Hanss, D. R. Bobbili, S. Bolognin, E. Glaab, K. Wolynska, N. Weisschuh, L. De Conti, C. May, F. Giesert, D. Grossmann, A. Lambert, S. Kirchen, M. Biryukov, L. F. Burbulla, F. Massart, J. Bohler, G. Cruciani, B. Schmid, A. Kurz-Drexler, P. May, S. Duga, C. Klein, J. C. Schwamborn, K. Marcus, D. Woitalla, D. M. V. Weisenhorn, W. Wurst, M. Baralle, D. Krainc, T. Gasser, B. Wissinger, R. Krüger, A patient-based model of RNA mis-splicing uncovers treatment targets in Parkinson's disease. *Sci. Transl. Med.* **12**, eaau3960 (2020).
21. M. Yoshida, N. Kataoka, K. Miyauchi, K. Ohe, K. Iida, S. Yoshida, T. Nojima, Y. Okuno, H. Onogi, T. Usui, A. Takeuchi, T. Hosoya, T. Suzuki, M. Hagiwara, Rectifier of aberrant mRNA splicing recovers tRNA modification in familial dysautonomia. *Proc. Natl. Acad. Sci. U.S.A.* **112**, 2764–2769 (2015).
22. A. Schaub, E. Glasmacher, Splicing in immune cells—mechanistic insights and emerging topics. *Int. Immunol.* **29**, 173–181 (2017).
23. L. B. Ivashkiv, IFN γ : Signalling, epigenetics and roles in immunity, metabolism, disease and cancer immunotherapy. *Nat. Rev. Immunol.* **18**, 545–558 (2018).
24. K. Dhatchinamoorthy, J. D. Colbert, K. L. Rock, Cancer immune evasion through loss of MHC class I antigen presentation. *Front. Immunol.* **12**, 636568 (2021).
25. B. Reynisson, B. Alvarez, S. Paul, B. Peters, M. Nielsen, NetMHCpan-4.1 and NetMHCIIpan-4.0: Improved predictions of MHC antigen presentation by concurrent motif deconvolution and integration of MS MHC eluted ligand data. *Nucleic Acids Res.* **48**, W449–W454 (2020).
26. B. J. Hos, M. G. M. Camps, J. van den Bulk, E. Tondini, T. C. van den Ende, D. Ruano, K. Franken, G. M. C. Janssen, A. Ru, D. V. Filippov, R. Arens, P. A. van Veelen, N. Miranda, F. Ossendorp, Identification of a neo-epitope dominating endogenous CD8 T cell responses to MC-38 colorectal cancer. *Oncotargets Ther.* **9**, 1673125 (2019).
27. Y. Takamiya, C. Schönbach, K. Nokihara, M. Yamaguchi, S. Ferrone, K. Kano, K. Egawa, M. Takiguchi, HLA-B*3501-peptide interactions: Role of anchor residues of peptides in their binding to HLA-B*3501 molecules. *Int. Immunol.* **6**, 255–261 (1994).
28. S. X. Lu, E. De Neef, J. D. Thomas, E. Sabio, B. Rousseau, M. Gigoux, D. A. Knorr, B. Greenbaum, Y. Elhanati, S. J. Hogg, A. Chow, A. Ghosh, A. Xie, D. Zamarin, D. Cui, C. Erickson, M. Singer, H. Cho, E. Wang, B. Lu, B. H. Durham, H. Shah, D. Chowell, A. M. Gabel, Y. Shen, J. Liu, J. Jin, M. C. Rhodes, R. E. Taylor, H. Molina, J. D. Wolchok, T. Merghoub,

- L. A. Diaz, O. Abdel-Wahab, R. K. Bradley, Pharmacologic modulation of RNA splicing enhances anti-tumor immunity. *Cell* **184**, 4032–4047.e31 (2021).
29. C. U. Blank, W. N. Haining, W. Held, P. G. Hogan, A. Kallies, E. Lugli, R. C. Lynn, M. Philip, A. Rao, N. P. Restifo, A. Schietinger, T. N. Schumacher, P. L. Schwartzberg, A. H. Sharpe, D. E. Speiser, E. J. Wherry, B. A. Youngblood, D. Zehn, Defining 'T cell exhaustion'. *Nat. Rev. Immunol.* **19**, 665–674 (2019).
 30. M. Sakuma, K. Iida, M. Hagiwara, Deciphering targeting rules of splicing modulator compounds: Case of TG003. *BMC Mol. Biol.* **16**, 16 (2015).
 31. L. Frankiw, D. Baltimore, G. Li, Alternative mRNA splicing in cancer immunotherapy. *Nat. Rev. Immunol.* **19**, 675–687 (2019).
 32. M. Seiler, S. Peng, A. A. Agrawal, J. Palacino, T. Teng, P. Zhu, P. G. Smith; Cancer Genome Atlas Research Network, S. Buonamici, L. Yu, Somatic mutational landscape of splicing factor genes and their functional consequences across 33 cancer types. *Cell Rep.* **23**, 282–296.e4 (2018).
 33. M. Ajiro, R. Jia, Y. Yang, J. Zhu, Z.-M. Zheng, A genome landscape of SRSF3-regulated splicing events and gene expression in human osteosarcoma U2OS cells. *Nucleic Acids Res.* **44**, 1854–1870 (2016).
 34. P. A. Ott, S. Hu-Lieskovan, B. Chmielowski, R. Govindan, A. Naing, N. Bhardwaj, K. Margolin, M. M. Awad, M. D. Hellmann, J. J. Lin, T. Friedlander, M. E. Bushway, K. N. Balogh, T. E. Sciuoto, V. Kohler, S. J. Turnbull, R. Besada, R. R. Curran, B. Trapp, J. Scherer, A. Poran, D. Harjanto, D. Barthelme, Y. S. Ting, J. Z. Dong, Y. Ware, Y. Huang, Z. Huang, A. Wanamaker, L. D. Cleary, M. A. Moles, K. Manson, J. Greshock, Z. S. Khondker, E. Fritsch, M. S. Rooney, M. DeMario, R. B. Gaynor, L. Srinivasan, A phase Ib trial of personalized neoantigen therapy plus anti-PD-1 in patients with advanced melanoma, non-small cell lung cancer, or bladder cancer. *Cell* **183**, 347–362.e24 (2020).
 35. E. Blass, P. A. Ott, Advances in the development of personalized neoantigen-based therapeutic cancer vaccines. *Nat. Rev. Clin. Oncol.* **18**, 215–229 (2021).
 36. N. A. Rizvi, M. D. Hellmann, A. Snyder, P. Kvistborg, V. Makarov, J. J. Havel, W. Lee, J. Yuan, P. Wong, T. S. Ho, M. L. Miller, N. Rekhtman, A. L. Moreira, F. Ibrahim, C. Bruggeman, B. Gasmir, R. Zappasodi, Y. Maeda, C. Sander, E. B. Garon, T. Merghoub, J. D. Wolchok, T. N. Schumacher, T. A. Chan, Mutational landscape determines sensitivity to PD-1 blockade in non-small cell lung cancer. *Science* **348**, 124–128 (2015).
 37. J. Zhu, T. Zhang, J. Li, J. Lin, W. Liang, W. Huang, N. Wan, J. Jiang, Association between tumor mutation burden (TMB) and outcomes of cancer patients treated with PD-1/ PD-L1 inhibitors: A meta-analysis. *Front. Pharmacol.* **10**, 673 (2019).
 38. Z. R. Chalmers, C. F. Connelly, D. Fabrizio, L. Gay, S. M. Ali, R. Ennis, A. Schrock, B. Campbell, A. Shlien, J. Chmielecki, F. Huang, Y. He, J. Sun, U. Tabori, M. Kennedy, D. S. Lieber, S. Roels, J. White, G. A. Otto, J. S. Ross, L. Garraway, V. A. Miller, P. J. Stephens, G. M. Frampton, Analysis of 100,000 human cancer genomes reveals the landscape of tumor mutational burden. *Genome Med.* **9**, 34 (2017).
 39. A. Kumar, K. Chamoto, P. S. Chowdhury, T. Honjo, Tumors attenuating the mitochondrial activity in T cells escape from PD-1 blockade therapy. *eLife* **9**, e52330 (2020).
 40. F. A. Ran, P. D. Hsu, J. Wright, V. Agarwala, D. A. Scott, F. Zhang, Genome engineering using the CRISPR-Cas9 system. *Nat. Protoc.* **8**, 2281–2308 (2013).
 41. M. B. Lutz, N. Kukutsch, A. L. J. Ogilvie, S. Röbner, F. Koch, N. Romani, G. Schuler, An advanced culture method for generating large quantities of highly pure dendritic cells from mouse bone marrow. *J. Immunol. Methods* **223**, 77–92 (1999).
 42. D. Kim, J. M. Paggi, C. Park, C. Bennett, S. L. Salzberg, Graph-based genome alignment and genotyping with HISAT2 and HISAT-genotype. *Nat. Biotechnol.* **37**, 907–915 (2019).
 43. K. L. Howe, P. Achuthan, J. Allen, J. Allen, J. Alvarez-Jarreta, M. Ridwan Amode, I. M. Armean, A. G. Azov, R. Bennett, J. Bhai, K. Billis, S. Boddu, M. Charkhchi, C. Cummins, L. da Rin, Fioretto, C. Davidson, K. Dodiya, B. El Houdaigui, R. Fatima, A. Gall, C. G. Giron, T. Grego, C. Guijarro-Clarke, L. Haggerty, A. Hemrom, T. Hourlier, O. G. Izuogu, T. Juettemann, V. Kaikala, M. Kay, I. Lavidas, T. Le, D. Lemos, J. G. Martinez, J. C. Marugán, T. Maurel, A. C. McMahon, S. Mohanan, B. Moore, M. Muffato, D. N. Oheh, D. Paraschas, A. Parker, A. Parton, I. Prosovetskaia, M. P. Sakhivel, A. I. Abdul Salam, B. M. Schmitt, H. Schuilenburg, D. Sheppard, E. Steed, M. Szpak, M. Szuba, K. Taylor, A. Thormann, G. Threadgold, B. Walts, A. Winterbottom, M. Chakiachvili, A. Chaubal, N. de Silva, B. Flint, A. Frankish, S. E. Hunt, G. R. Ilesley, N. Langridge, J. E. Loveland, F. J. Martin, J. M. Mudge, J. Morales, E. Perry, M. Ruffier, J. Tate, D. Thybert, S. J. Trevanion, F. Cunningham, A. D. Yates, D. R. Zerbino, P. Flicek, Ensembl 2021. *Nucleic Acids Res.* **49**, D884–D891 (2021).
 44. S. Shen, J. W. Park, Z.-X. Lu, L. Lin, M. D. Henry, Y. N. Wu, Q. Zhou, Y. Xing, rMATS: Robust and flexible detection of differential alternative splicing from replicate RNA-Seq data. *Proc. Natl. Acad. Sci. U.S.A.* **111**, E5593–E5601 (2014).
 45. C. Trapnell, B. A. Williams, G. Pertea, A. Mortazavi, G. Kwan, M. J. Van Baren, S. L. Salzberg, B. J. Wold, L. Pachter, Transcript assembly and quantification by RNA-Seq reveals unannotated transcripts and isoform switching during cell differentiation. *Nat. Biotechnol.* **28**, 511–515 (2010).
 46. S. Uzor, S. R. Porazinski, L. Li, B. Clark, M. Ajiro, K. Iida, M. Hagiwara, A. A. Alqasem, C. M. Perks, I. D. Wilson, S. Oltean, M. R. Ladomery, CDC2-like (CLK) protein kinase inhibition as a novel targeted therapeutic strategy in prostate cancer. *Sci. Rep.* **11**, 7963 (2021).
 47. B. Li, C. N. Dewey, RSEM: Accurate transcript quantification from RNA-Seq data with or without a reference genome. *BMC Bioinformatics* **12**, 323 (2011).
 48. M. I. Love, W. Huber, S. Anders, Moderated estimation of fold change and dispersion for RNA-seq data with DESeq2. *Genome Biol.* **15**, 550 (2014).
- Acknowledgments:** We appreciate members of the Department of Anatomy and Developmental Biology and the Department of Drug Discovery Medicine of Kyoto University Graduate School of Medicine for fruitful discussions, the Center for Anatomical, Pathological and Forensic Medical Research of Kyoto University Graduate School of Medicine for preparing microscope slides, K. Makigaya of Kyoto University for technical assistance, and M. Takiguchi of Kumamoto University for providing B2M-introduced RMA-S cells. **Funding:** This work was supported by Grants-in-Aid for Scientific Research by Japan Society for Promotion of Science 15H05721 (to M.H., K.I., and M.A.), 19K07367 (to M.A.), and 21H05042 (to M.H. and M.A.). **Author contributions:** M.A., K.C., T.H., and M.H. conceptualized the study. S.M. and M.A. designed the experiments. S.M., M.A., and K.I. performed the investigations, statistical analysis, and visualization. K.I. mainly performed RNA-seq data processing and analysis to identify splice-neoantigen candidates. S.M., M.A., and M.H. prepared the manuscript. All authors provided critical feedback and helped shape the research, analysis, and manuscript. **Competing interests:** S.M. is an employee of Kyorin Pharmaceutical Co. Ltd. M.H. is a founder, shareholder, and member of the scientific advisory board of KinoPharma Inc., and BTB Drug Development Research Center Co. Ltd. The remaining authors declare that they have no competing interests. **Data and materials availability:** All data associated with this study are in the paper or the Supplementary Materials. Correspondence and requests for materials should be addressed to M.H. RECTAS is available from M.H. for research purposes under a material transfer agreement with Kyoto University. The RNA-seq data generated in this study have been deposited in the Gene Expression Omnibus (accession nos. GSE183981 and GSE205137).
- Submitted 8 December 2021
Resubmitted 22 June 2022
Accepted 24 October 2022
Published 30 November 2022
10.1126/scitranslmed.abn6056

Chemical induction of splice-neoantigens attenuates tumor growth in a preclinical model of colorectal cancer

Shingo Matsushima, Masahiko Ajiro, Kei Iida, Kenji Chamoto, Tasuku Honjo, and Masatoshi Hagiwara

Sci. Transl. Med., **14** (673), eabn6056.

DOI: 10.1126/scitranslmed.abn6056

Splice and dice

Cancer immunotherapy is most effective when neoantigens are present at high abundance. However, some types of cancer do not have a high tumor mutational burden and thus do not have many neoantigens. Here, Matsushima *et al.* used an alternative approach to generate neoantigens. The authors chemically induced splice-neoantigens in mice with colorectal cancer using a synthetic compound called RECTAS. RECTAS treatment suppressed tumor growth in a CD8+ T cell–dependent manner and also enhanced immune checkpoint blockade. Together, these results suggest that splicing modulators merit further investigation as part of the cancer immunotherapy toolbox.—CM.

View the article online

<https://www.science.org/doi/10.1126/scitranslmed.abn6056>

Permissions

<https://www.science.org/help/reprints-and-permissions>

Use of this article is subject to the [Terms of service](#)

Science Translational Medicine (ISSN) is published by the American Association for the Advancement of Science, 1200 New York Avenue NW, Washington, DC 20005. The title *Science Translational Medicine* is a registered trademark of AAAS.

Copyright © 2022 The Authors, some rights reserved; exclusive licensee American Association for the Advancement of Science. No claim to original U.S. Government Works

Supplementary Materials for
**Chemical induction of splice-neoantigens attenuates tumor growth in a
preclinical model of colorectal cancer**

Shingo Matsushima *et al.*

Corresponding author: Masahiko Ajiro, ajiro.masahiko.6e@kyoto-u.ac.jp;
Masatoshi Hagiwara, hagiwara.masatoshi.8c@kyoto-u.ac.jp

Sci. Transl. Med. **14**, eabn6056 (2022)
DOI: 10.1126/scitranslmed.abn6056

The PDF file includes:

Figs. S1 to S11
Legends for data files S1 to S6

Other Supplementary Material for this manuscript includes the following:

MDAR Reproducibility Checklist
Data files S1 to S6

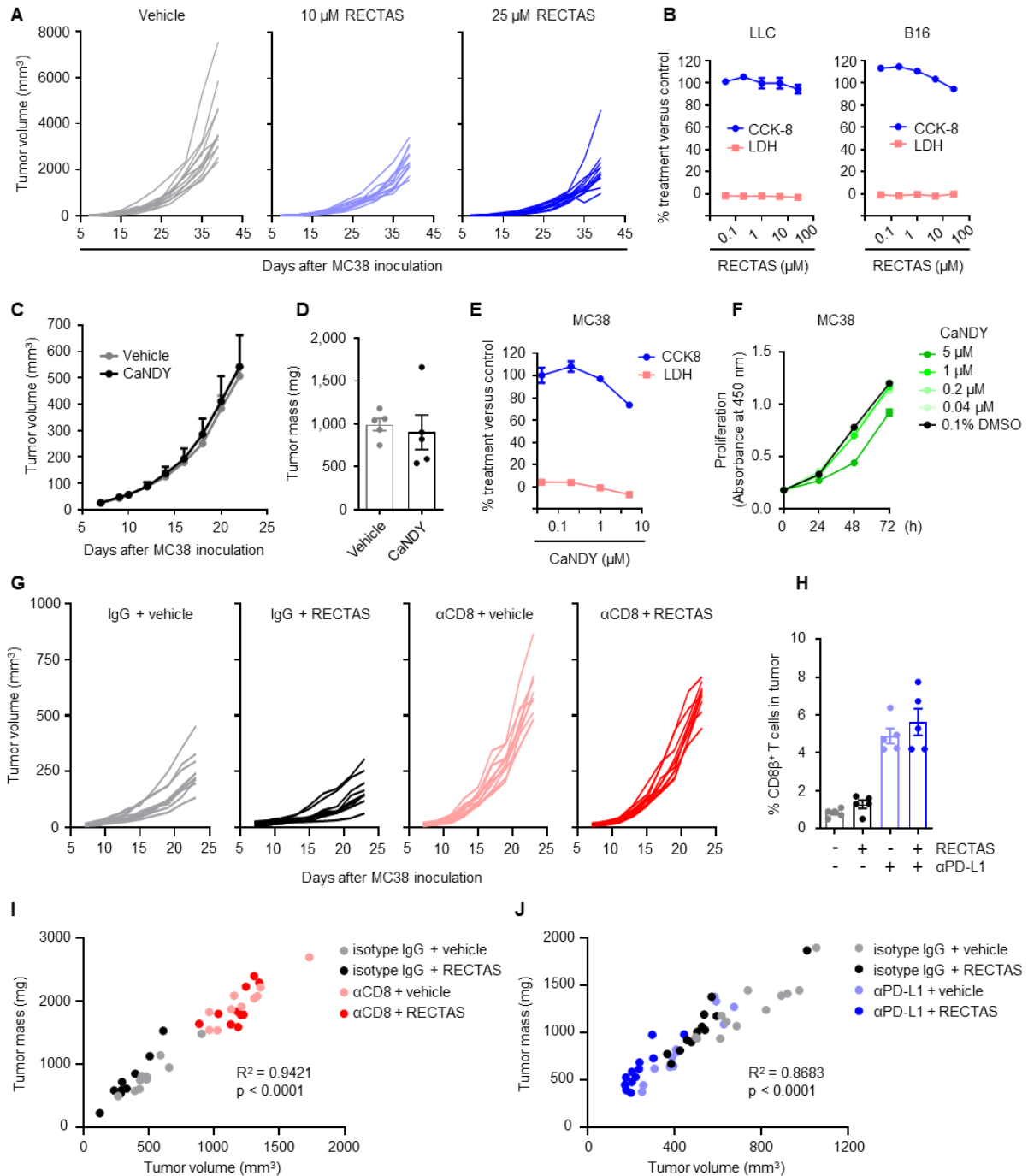


Fig. S1. Antitumor effects of rectifier of aberrant splicing (RECTAS) and CDC37 association inhibitor for DYRK1A (CaNDY) in vivo and in vitro.

In an MC38 tumor-bearing model, mice were treated intratumorally with test substances or vehicle control (0.1% dimethyl sulfoxide, DMSO) once daily when the tumor volume reached 30 to 50

mm³. **(A)** Spider plots showing individual tumor growth are shown (n = 12 per group), related to Fig. 1B. **(B)** Cell proliferation and cell death were measured using the Cell Counting Kit-8 (CCK-8) and lactate dehydrogenase (LDH) assays, respectively (n = 3 per group). The murine Lewis lung carcinoma (LLC) and B16 melanoma cell lines were treated with either RECTAS (0.04, 0.2, 1, 5, or 25 μ M) or 0.1% DMSO for 72 hours. **(C and D)** Tumor volumes (C) and masses (D) are shown (n = 5 per group). Mice were treated with 1 μ M CaNDY or vehicle. **(E and F)** MC38 cells were treated with either CaNDY (0.04, 0.2, 1, or 5 μ M) or 0.1% DMSO. **(E)** CCK-8 and LDH assays for MC38 cells at 72 hours following CaNDY treatment are shown. **(F)** Growth curves are shown for MC38 cells treated with CaNDY for indicated time points. **(G)** Spider plots (n = 12 per group) are shown, related to Fig. 1M. **(H)** Tumor-infiltrating CD8⁺ T cells (n = 5 per group) were quantified on day 14 following MC38 inoculation. Mice were intraperitoneally injected with anti-programmed cell death ligand 1 (α PD-L1) antibody (35 μ g) or isotype IgG on day 7. **(I and J)** Scatter plots are shown representing the correlation between tumor masses and volumes on day 23 (n = 10 or 12 per group for (I) or (J), respectively), related to Fig. 1, M and O. Data are shown as the mean \pm SEM for (B) to (F), and (H). Experiments were performed at least twice for (A), (B), (G), (I), and (J), or once for others.

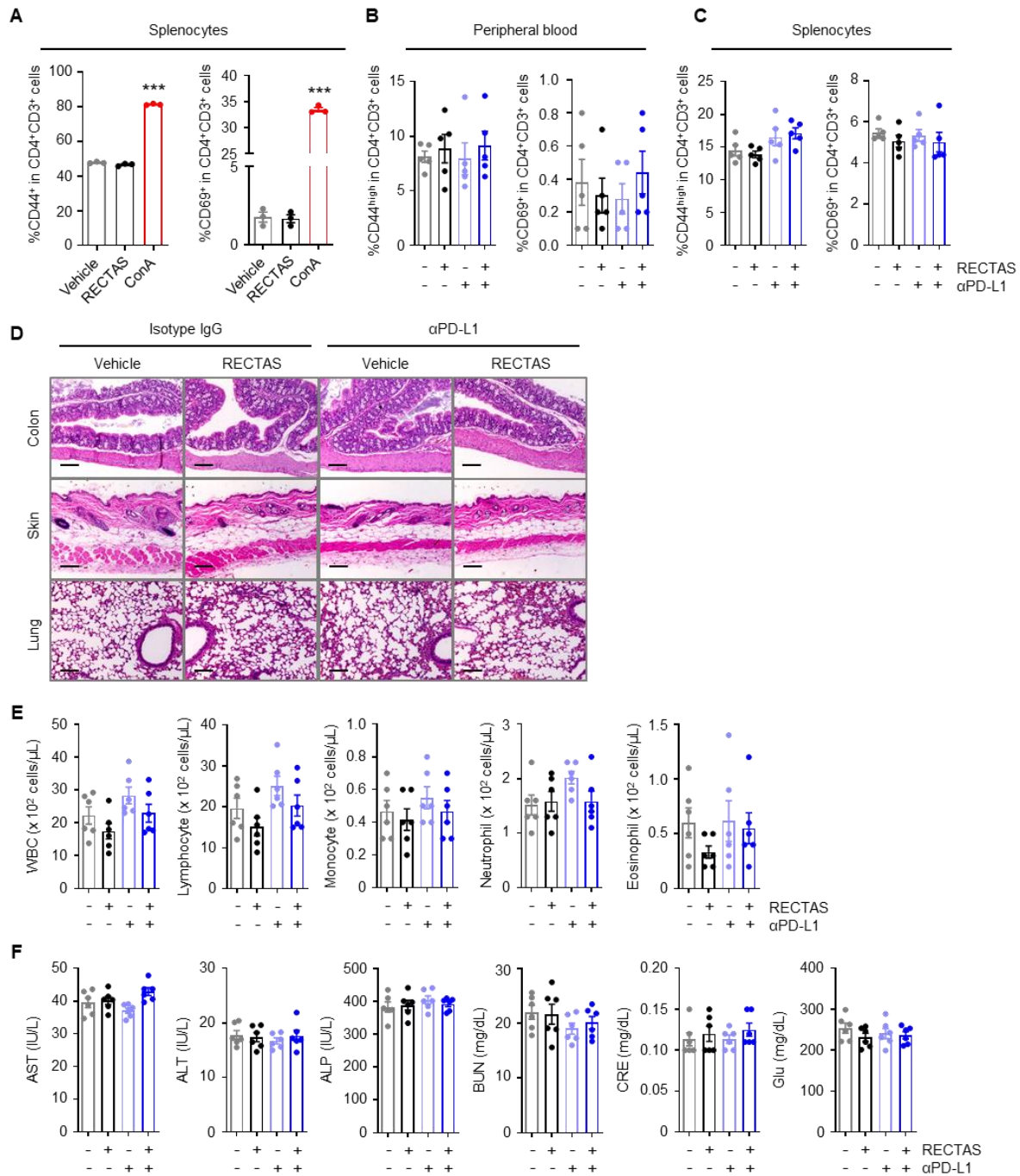


Fig. S2. Evaluation of RECTAS for autoimmune responses.

(A) Splenocytes were prepared from 8-week-old female C57BL/6N mice and treated with RECTAS (10 μM) or vehicle control (0.1% DMSO) for 24 hours. Concanavalin A (ConA) was used as a positive control. Frequencies of CD44⁺ and CD69⁺ among CD4⁺ T cells in groups with

the indicated treatments (n = 3 per group). ***, p<0.001 versus vehicle was determined using one-way ANOVA followed by Bonferroni's multiple-comparison test. **(B to F)** RECTAS (100 mg/kg) or vehicle control (0.5% CMC-Na) was orally administered to 7-week-old female C57BL/6N mice twice daily for 7 consecutive days (B and C) or once daily for 4 weeks (D to F), while α PD-L1 antibody (35 μ g) or isotype control was intraperitoneally injected once weekly. Frequencies of CD44^{high} and CD69⁺ among CD4⁺ T cells in peripheral blood (B) and spleen (C) on day 7 are shown (n = 5 per group). Representative images of the tissue sections (colon, skin, and lung) with hematoxylin and eosin (H&E) staining on day 28 are indicated in (D). Scale bars: 100 μ m. White blood cell (WBC) numbers and biochemical parameters in peripheral blood on day 28 (n = 6/group) are respectively shown in (E) and (F). AST, aspartate aminotransferase; ALT, alanine aminotransferase; ALP, alkaline phosphatase; BUN, blood urea nitrogen; CRE, creatinine; Glu, glucose. All data are shown as the mean \pm SEM. Experiments were performed at least twice for (A), or once for others.

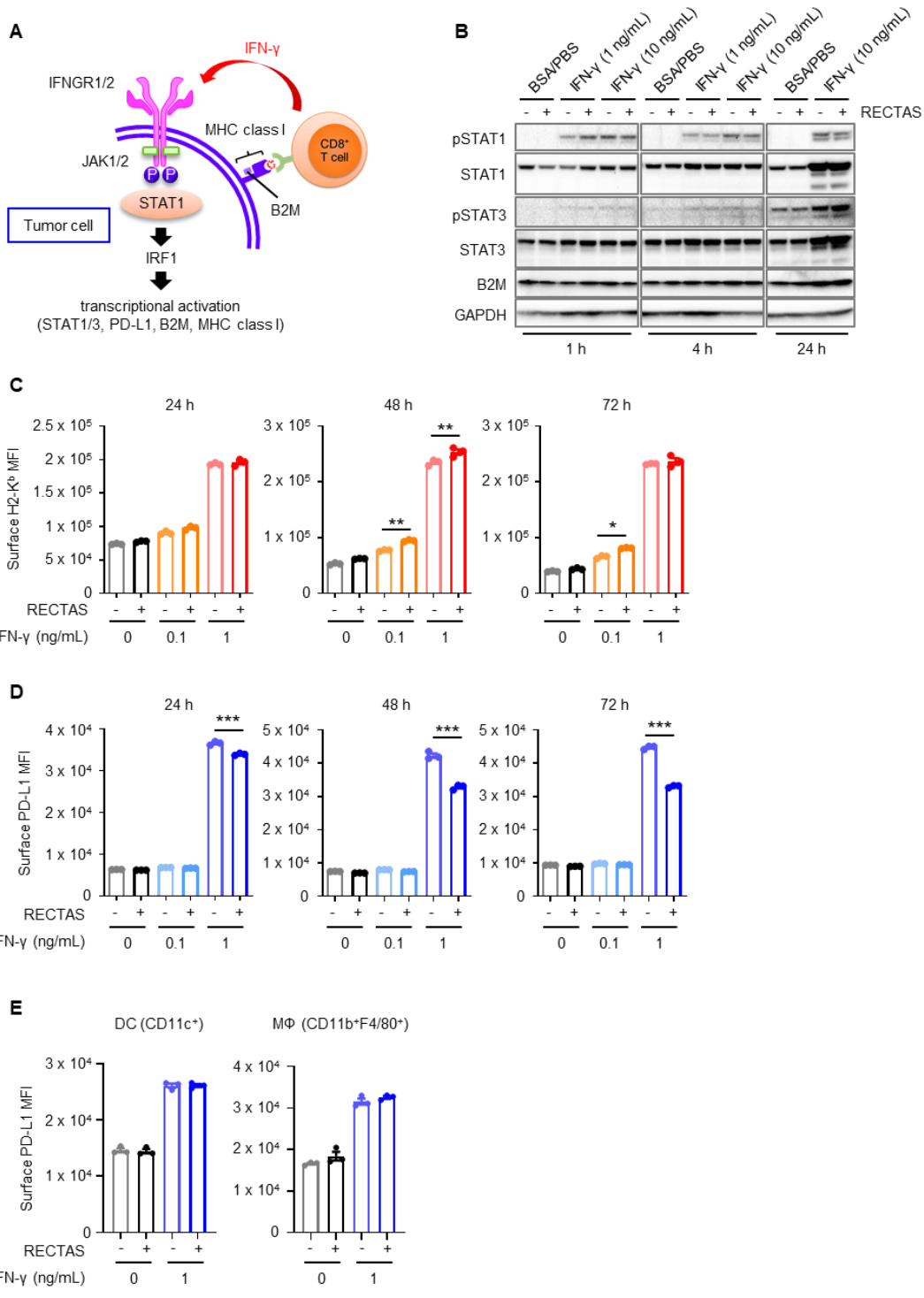


Fig. S3. Interferon (IFN)- γ signaling in cancer cells treated with RECTAS.

(A) Diagram illustrating the IFN- γ signaling and major histocompatibility complex (MHC) class I pathway in cancer cells. IFNGR, IFN- γ receptor; B2M, β 2 microglobulin; JAK, Janus tyrosine kinase; STAT, signal transducer and activator of transcription; IRF, interferon-regulatory factor.

(B to D) MC38 cells were pretreated with 10 μ M RECTAS for 48 hours, followed by treatment with IFN- γ at indicated concentrations and time points. (B) Indicated proteins were detected using western blotting. GAPDH served as the loading control. BSA/PBS, bovine serum albumin plus phosphate buffered saline. The expression of surface H2-K^b (C) and PD-L1 (D) was measured through flow cytometry. MFI, median fluorescence intensity. *, $p < 0.05$; **, $p < 0.01$; ***, $p < 0.001$ as determined using one-way ANOVA followed by Bonferroni's multiple-comparison test.

(E) The expression of surface PD-L1 was measured by flow cytometry in dendritic cells (DC; CD11c⁺) and macrophages (M Φ ; CD11b⁺F4/80⁺) derived from splenocytes pretreated with 10 μ M RECTAS or 0.1% DMSO for 24 hours, followed by 1 ng/mL IFN- γ for a further 24 hours. All data are shown as the mean \pm SEM ($n = 3$ per group). All experiments were performed once.

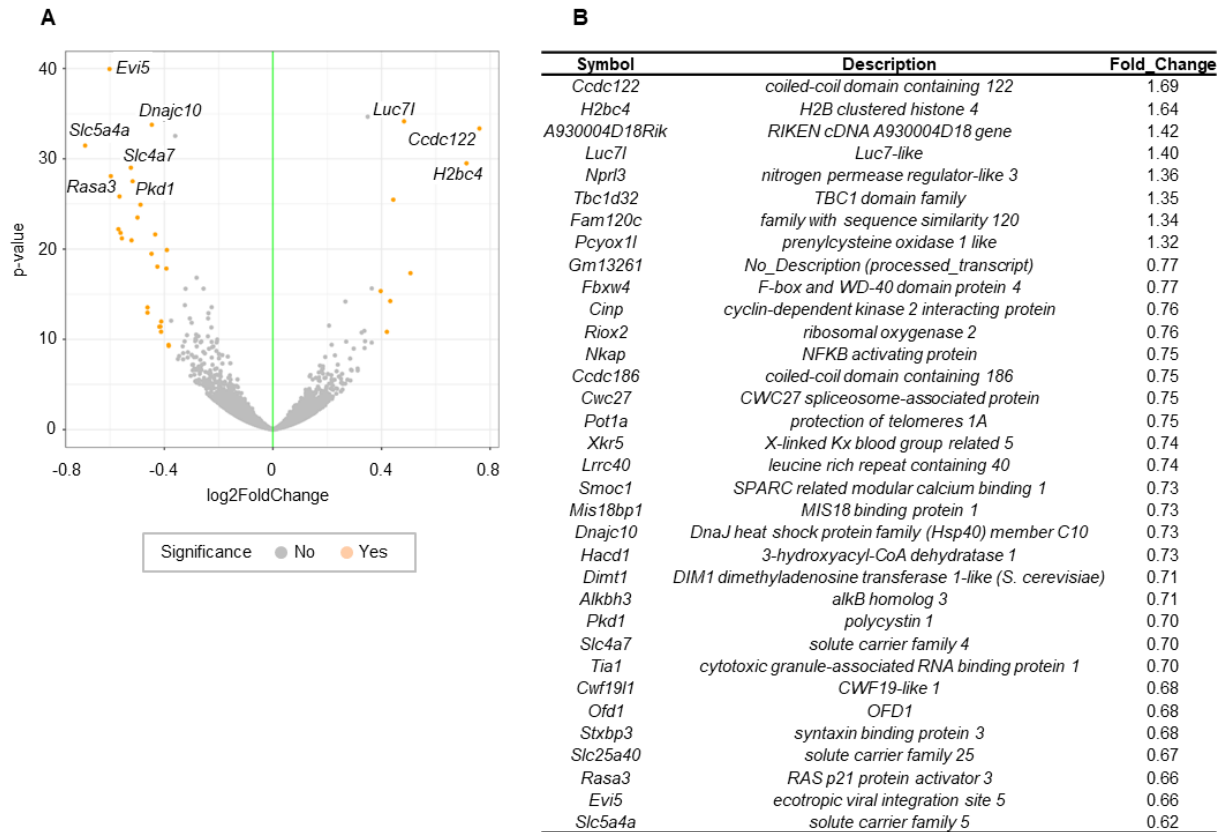


Fig. S4. Differentially expressed gene (DEG) analysis in MC38 cells with RECTAS.

(A and B) Total RNA was prepared from MC38 cells in three biological replicates after treatment with 10 μ M RECTAS or 0.1% DMSO for 6 hours; extracted RNA was subjected to RNA-seq analysis. For DEG analysis, transcripts per million (TPM) values and raw read counts were calculated. Then, the DESeq2 program was employed to identify DEGs using the following criteria: adjusted p-value < 0.05, fold-change ≥ 1.3 or $\leq 1/1.3$, average TPM ≥ 1 , and average raw-read counts ≥ 32 in at least a replicate. Significantly altered genes and values of fold-change are shown in the volcano plot (A) and table (B), respectively.

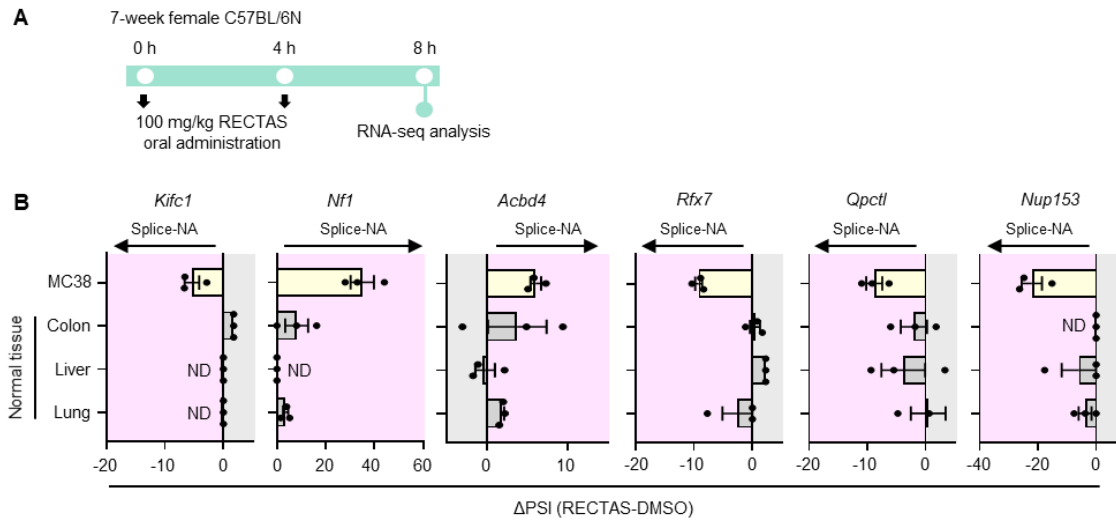


Fig. S5. Splice-neoantigen forms with RECTAS in non-malignant tissues.

(A) A scheme of the experiment for RNA-seq analysis of non-malignant tissues from normal mice. RECTAS (100 mg/kg) or vehicle control (0.5% CMC-Na) was orally administered to 7-week-old female C57BL/6N mice as described in the scheme (n = 3 per group). Four hours after the second administration, tissues (colon, liver, and lung) were collected and stored at -80°C until use. Extracted total RNAs from these tissues were subjected to RNA-seq analysis. (B) Splice-neoantigen producing rates calculated from RNA-seq data (n = 3 biological replicates per group) are indicated as the difference in values of percent spliced in (Δ PSI; RECTAS – DMSO). Data are shown as the mean \pm SEM. ND, not detected.

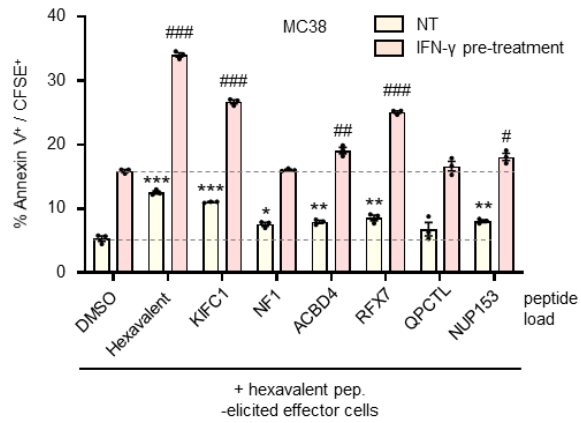


Fig. S6. In vitro tumor-killing activity mediated by individual splice-neoantigens.

Quantitative data of carboxyfluorescein succinimidyl ester (CFSE)⁺/Annexin V⁺ frequency is indicated (n = 3 per group). CFSE-labeled MC38 cells, with or without IFN- γ pretreatment, were further stimulated with either 0.1% DMSO, hexavalent peptides, or individual peptides for 2 hours, and then cocultured with hexavalent peptides-reactive effector cells for 24 hours. NT, not treated. * or #, p < 0.05; ** or ##, p < 0.01; *** or ###, p < 0.001 versus corresponding DMSO controls as determined using an unpaired Student's *t*-test. Data are shown as the mean \pm SEM. The experiment was performed at least twice.

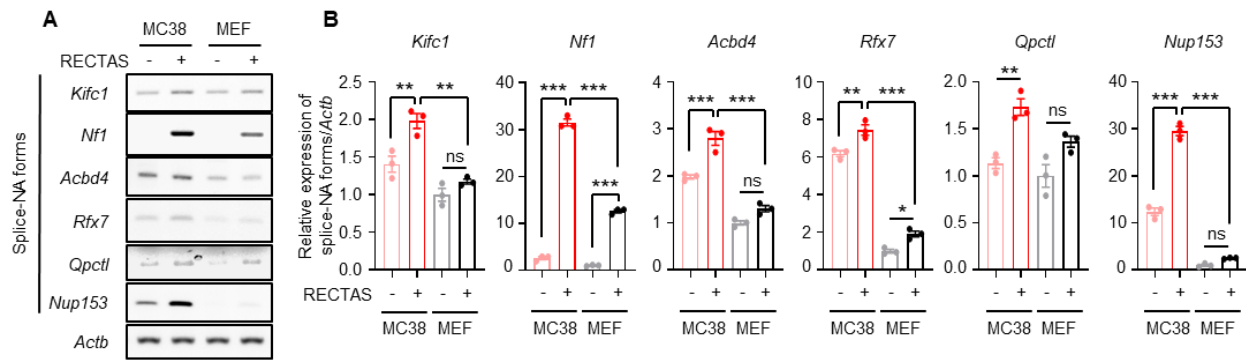


Fig. S7. Splice-neoantigen forms with RECTAS in mesenchymal embryonic fibroblasts (MEFs).

(**A** and **B**) RT-PCR analysis for splice-neoantigen coding forms (splice-NA forms) in MC38 cells and MEFs treated with 10 μ M RECTAS or vehicle control (0.1% DMSO) for 6 hours. Gel images (**A**) and quantification data (**B**) are shown (n = 3). *Actb* served as a loading control. *, p < 0.05; **, p < 0.01; ***, p < 0.001 as determined using an unpaired Student's *t*-test. ns, not significant.

Data are shown as the mean \pm SEM. The experiment was performed at least twice.

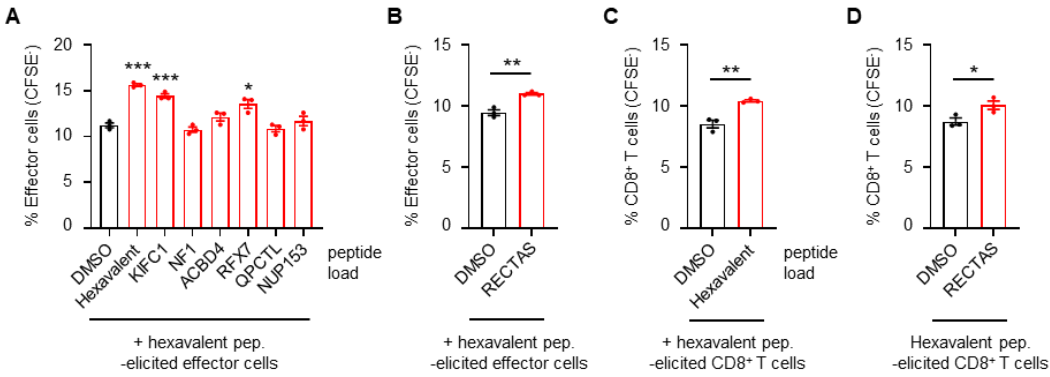


Fig. S8. Effector cell expansion when cocultured with MC38 cells.

Quantitative data of CFSE⁻ frequency is indicated (n = 3 per group). (A and B) Hexavalent peptides-elicited splenic effector cells were cocultured with CFSE-labelled MC38 cells stimulated with DMSO control, indicated peptides, or 25 μ M RECTAS for 24 hours. (C and D) CD8⁺ T cells were purified using a CD8 α ⁺ T cell isolation kit from splenic effector cells prior to coculture with MC38 cells, and a coculture assay for tumor lysis was performed as described in (A and B). *, p < 0.05; **, p < 0.01; ***, p < 0.001 versus corresponding DMSO controls as determined using an unpaired Student's *t*-test. Data are shown as the mean \pm SEM. Experiments were performed at least twice for (A and B), or once for (C and D).

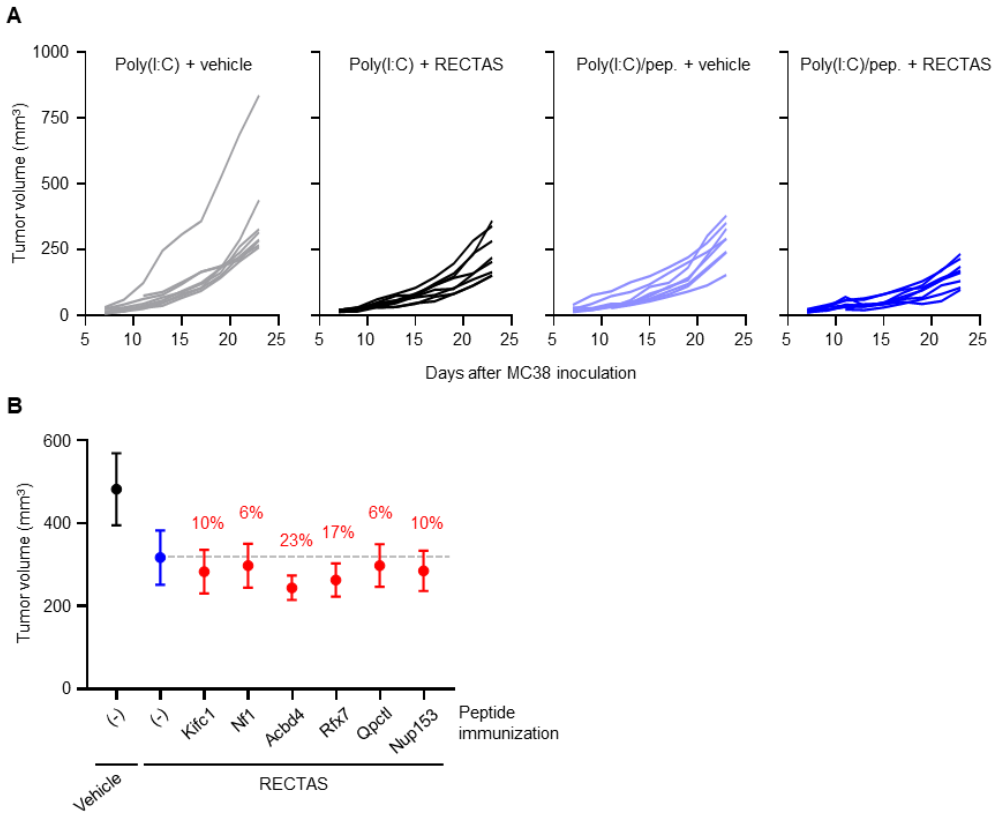


Fig. S9. Tumor suppressive effect by hexavalent or individual splice-neoantigen vaccination.

(A) Spider plots (n = 8 per group) are shown, related to Fig. 6J. (B) Tumor volumes of mice on day 23 are shown. Mice were subcutaneously vaccinated with 100 µg of peptide and 50 µg of Poly(I:C) on day 11 and 18. In groups shown as (-), 5% DMSO was injected instead of peptide. RECTAS (10 µM) or vehicle control (0.1% DMSO) was intratumorally given once daily. Data are shown as the mean ± SEM (n = 7 per group). Experiments were performed once.

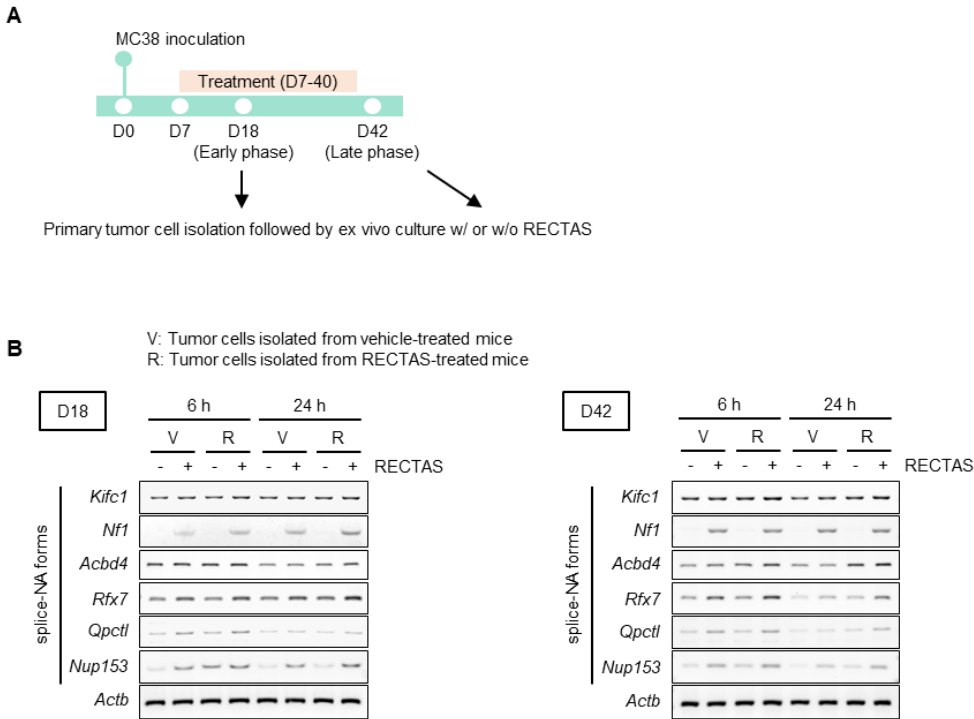


Fig. S10. Characterization of cancer cell immune selection.

(A) Scheme of long-term treatment with RECTAS in MC38 tumor-bearing model followed by tumor cell isolation and analysis. RECTAS (10 μ M) or vehicle control (0.1% DMSO) was intratumorally administered to mice once daily (day 7 to 40). Primary cancer cells were isolated from implanted tumor of mice on day 18 (early phase) and 42 (late phase) using a tumor dissociation and isolation kit. Isolated cancer cells were plated on dishes and treated with 10 μ M RECTAS or 0.1% DMSO for 6 or 24 hours. Total RNA was extracted from these treated cancer cells for RT-PCR analysis. (B) Gel images obtained from RT-PCR analysis for splice-neoantigen coding forms (splice-NA forms) are shown. *Actb* served as a loading control. The experiment was performed once.

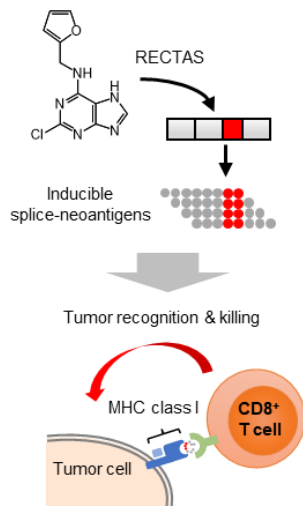


Fig. S11. Diagrammatic summary of this study.

The synthetic splicing modifier, RECTAS, sensitively creates nonannotated irregular splice junctions in cancer cells. Immunogenic peptides translated from these splice-neoepitopes function as genuine neoantigens mediating antitumor immune responses.

Data file S1. Safety assessment in mice with chronic treatment of RECTAS.

Data file S2. List of RECTAS-inducible splice-neoantigen candidates in MC38 cells.

Data file S3. Curated list of RECTAS-inducible 22 splice-neoantigen candidates in MC38 cells.

Data file S4. Splicing profiles affected by RECTAS in normal tissues.

Data file S5. List of oligonucleotide used in this study.

Data file S6. Raw data for all experiments in this study.